1983

NMR study of molecular motions in two disordered organic solids

Philip L. Kuhns
College of William & Mary - Arts & Sciences

Kuhns, Philip Laurence

NMR STUDY OF MOLECULAR MOTIONS IN TWO DISORDERED ORGANIC SOLIDS

The College of William and Mary in Virginia PH.D. 1983

PLEASE NOTE:

In all cases this material has been filmed in the best possible way from the available copy. Problems encountered with this document have been identified here with a check mark ✓.

1. Glossy photographs or pages _____
2. Colored illustrations, paper or print _____
3. Photographs with dark background _____
4. Illustrations are poor copy _____
5. Pages with black marks, not original copy _____
6. Print shows through as there is text on both sides of page _____
7. Indistinct, broken or small print on several pages ✓
8. Print exceeds margin requirements _____
9. Tightly bound copy with print lost in spine _____
10. Computer printout pages with indistinct print _____
11. Page(s) _____ lacking when material received, and not available from school or author.
12. Page(s) _____ seem to be missing in numbering only as text follows.
13. Two pages numbered _____. Text follows.
14. Curling and wrinkled pages _____
15. Other _____

University Microfilms International

NMR STUDY OF MOLECULAR MOTIONS IN TWO DISORDERED ORGANIC SOLIDS

A Dissertation

Presented to

The Faculty of the Department of Physics

The College of William and Mary in Virginia

In Partial Fulfillment

Of the Requirements for the Degree of

Doctor of Philosophy

---

by

Philip L. Kuhns

October 1983

NMR STUDY OF MOLECULAR MOTIONS IN TWO DISORDERED ORGANIC SOLIDS

APPROVAL SHEET

This dissertation is submitted in partial fulfillment

of the requirements of the degree of

Doctor of Philosophy

Philip Kuhns

Philip L. Kuhns

Approved, October 1983

Mark S. Conradi

Mark S. Conradi

Roy L. Champion

Roy L. Champion

William J. Kossler

William J. Kossler

Henry Krakauer

Henry Krakauer

Kenneth G. Petzinger

Kenneth G. Petzinger

David W. Thomson

David W. Thomson
Chemistry

ABSTRACT

The molecular motions are studied in two disordered materials that undergo glass transitions. Glycerol is a conventional glass former and cyclohexanol is an orientational glass former.

The technique used in the glycerol experiments was spectral hole burning. Chemical shift anisotropy produces inhomogeneous broadening of NMR lines in orientationally disordered and polycrystalline solids. By saturating or inverting a portion of the anisotropic line, 'burning a hole,' molecules of certain orientations are tagged. Subsequent molecular reorientations result in spectral diffusion which is not related to spin-spin interactions. By measuring the broadening and recovery of the hole as a function of time, detailed knowledge of the reorientation is obtained. For example, the mean jump rate and the lower limit of angular reorientations are determined. The reorientation rate in supercooled glycerol is followed from $10^{-2} s^{-1}$ to 10^{2} s^{-1} Our measurements agreed with previous results and extended them to lower frequencies. The mean jump size was determined to be greater than 45 degrees. The hole recovery curves were not exponential, but were fitted with the Williams-Watts function, exp = $(\tau/\tau_0)^{\beta}$ with $\beta = 0.5$.

The motions in the rotor phase of solid cyclohexanol are studied with proton NMR from the melt down to 5 K. Particular attention is paid to the variation of the linewidth with temperature and to the temperature and frequency dependences of T_1. We find there are two distinct motions that cause minima in T_1 as a function of temperature. These two motions were observed in dielectric experiments. From the proton line narrowing and C^{13} high-resolution solid state spectra, the high temperature 'α' motion is identified as overall molecular rotation. The low temperature 'β' motion is identified as a uniaxial internal rotation of the cyclohexyl ring about the CO bond, with the COH group remaining stationary . This explains both the strong spin relaxation and the weak dielectric relaxation peak associated with the β motion. Both motions have distributions of correlation times, as seen from the shallow T_1 minima and the weak temperature and frequency dependences of T_1. From 100 K down to 5 K, the temperature dependence continues to be weak. The frequency dependence remains less than ω_0^2. These results indicate that some components of the motion remain faster than the NMR frequency ω_0 even at 5 K. The behavior of cyclohexanol is compared to that of other disordered solids.

ACKNOWLEDGEMENTS

I would like to thank my advisor Mark Conradi for his infectious enthusiasm for physics, NMR and 'how does it work', his accessibility and friendship and, of course, for his lasagna. I would also like to thank those who went out of their way to make my stay at William and Mary a pleasant one. Donald Joyce, who donated and explained the Script program and his Spinmath package, extended his sympathy in the basement of Jones and his hospitality at Burkes pond. William Vulcan who answered my questions about electronics and came up with the required component to fix the spectrometer when it was down. Sylvia Stout for years of helpful direction and seeing to the steady supply of my habit, over 5,000 cups of hot, delicious coffee. Finally, my wife Faith who always encourged me to continue, provided the necessary levity when I was depressed and made me get out of bed each morning. On the commercial side of things, Howard Johnsons management and staff for many a cup of coffee and conversation when the rest of Williamsburg slept.

CONTENTS

Chapter I

INTRODUCTION

Nuclear Magnetic Resonance has been used to study molecular motions in liquids and solids since the pioneering NMR work of the 1940s. Indeed, it is the presence of molecular motions in nonconducting samples that gives rise to polarization of spins by the DC magnetic field, a basic requirement of NMR.

Reported here are results of NMR studies of the molecular motions in two organic materials that undergo glass transitions, glycerol and cyclohexanol.

Glycerol ($CH_2OH - CHOH - CH_2OH$) at low temperatures is a 'liquid' glass, a material that is both translationally and orientationally disordered and appears, macroscopically, to be solid. When liquid glycerol is cooled, the translational and orientational correlation times become longer, until near 185 K a glass transition is observed in the specific heat (Gib23). This indicates that the correlation times pass through 10^3 s. As glycerol is cooled from a liquid to below the glass transition it retains the orientational and translational disorder that characterizes the liquid state. Indeed, the only difference between liquid and glass is the time scale on which the molecules reorient and diffuse.

Above the glass transition temperature T_g, the motions are faster than laboratory time scales (10^3 s), and below T_g the motions are

slower than 10^3 s. Clearly, different measurement techniques have different inherent time scales and will measure different glass transition temperatures. The T_g in the literature always refers to slow thermodynamic and thermal expansion measurements.

Cyclohexanol ($C_6H_{11}OH$) freezes at 299 K into a rotor crystal (Ada68), a solid that has a crystal lattice (fcc, Z = 4 and a_o = 0.88 nm) (Cec80, Gre69, Dvn61), but retains the fast overall molecular rotation and the orientational disorder characteristic of a liquid. These kinds of solids, called plastic crystals, have been widely studied in the past. (Tim61, Bod76) With further cooling, at 265 K cyclohexanol passes a transition to a more ordered phase that can be easily avoided by supercooling (Ada77). Additional cooling slows the molecular reorientations in the supercooled rotor crystal. Near 150 K a glass transition occurs in which the overall molecular rotations freeze out. However an internal motion, rotation of the cyclohexyl ring about the CO bond with the COH group held fixed, persists below the glass transition.

A glass transition is a kinetic phenomenon whose signature in calorimetric studies is a step-like change in the specific heat (Gib23). The change is due to the freezing out of the glassing coordinate(s) that occurs over a narrow temperature range (~ 5 K). The temperature at which this change in the specific heat occurs is found to depend on the experimental equilibration time, the time in which the sample reaches a uniform temperature or the time between application of the heat pulse and the reading of the temperature change. Longer equilibration times allow slower motions to fulfill the criterion defining a 'fast' motion. The criterion is that the correlation time of the motion be less than

the equilibration time. Hence for longer equilibration times the temperature range over which the change in the specific heat occurs shifts to lower temperatures. What that means is that we have a time-dependent heat capacity.

The dependence on the equilibration time of the step-like change in the specific heat is one signature used to differentiate between kinetic glass transitions and conventional transitions. For ordinary transitions, such as those occuring in equilibrium statistical mechanics, time does not play any role. The glass transition temperature, T_g, is taken as the temperature where the specific heat is halfway down the step in the specific heat curve for long (10^3 s) equilibration times.

Our NMR study of the slow molecular reorientations in glycerol used a new slow motion technique, spectral hole-burning (Con81, Kuh82), that was developed at this laboratory. This technique exploits the existence of an anisotropic chemical shift to tag and subsequently follow slow molecular reorientations.

Spectral hole-burning yields detailed information about molecular reorientations, such as the width of the distribution of correlation times, the mean correlation time, and the angular size of single reorientations. In other words, spectral hole-burning yields the distribution of single-particle, two-time correlation functions for molecular reorientations. This is a much more detailed specification of the motion than is possible by using other relaxation techniques, such as determining T_1 or $T_{1\rho}$ using conventional NMR techniques or dielectric spectroscopy. Unless the electrons (and hence the molecule) have a

high degree of symmetry, the chemical shift will be anisotropic. That is, the size of the shift will depend on molecular orientation. Spectral hole-burning should be a widely applicable technique because many solid organic materials exhibit chemical shift anisotropy. The NMR study of the molecular motions in solid cyclohexanol used the techniques of nuclear relaxation spectroscopy (Noa71), which date back to the earliest days of NMR. These techniques use the fact that nuclear spin systems, having well defined energy levels, will undergo transitions only in response to perturbations at the frequency f, where $hf = \Delta E = \hbar\gamma H$. Perturbations due to molecular motions, which tend to restore equilibrium, cause changes in the populations of the magnetic energy levels. So the time constant associated with the return of these populations to thermal equilibrium will depend on the molecular motions. In particular, relaxation times will depend on the motional correlation rates, the width and shape of the distribution of correlation rates, the type of motion causing the perturbations, and the strength of the internal magnetic interaction being modulated. By changing the magnetic field, the frequencies ($f = \gamma H/2\pi$) being studied will be varied. This is analogous to varying a tuneable filter to investigate the intensity of a signal as a function of frequency. Here the 'signal' is from the random molecular motions.

The study of molecular motions near the glass temperature in disordered materials is important to understand the nature of glasses and glass transitions. Detailed theories explaining glasses and the glass transition are in their infancy because both detailed experimental and theoretical studies of glassing materials have only recently begun,

and because the periodicity exploited in theories of crystalline materials is not present in most glassing materials. The formation of a glass depends on the anisotropic part of the intermolecular potential. (Consider that spherically symmetric molecules such as Ar, Kr, Ne, and pure elemental metals do not form glasses.) The importance of the anisotropic intermolecular potentials makes calculations of the molecular motions in glasses difficult. In contrast, calculations for liquids and gases show that the symmetric part of the intermolecular potential dominates the behavior.

The study of molecular motions is important in understanding the bulk properties of glasses, such as plastics, that are used widely in everyday life. The manufacturing of products using plastics is often motivated by the ability to mold the viscous liquid and then cool it below the glass transition, and by the ability of the product to absorb bends and shocks, properties that seem to be related to the disorder in glasses.

Chapter II

THEORY: A SKETCH

NMR is the measurement of nuclear magnetization and its frequency distribution among interacting magnetic dipoles that have been placed in a large magnetic field. The magnetic field experienced by a nucleus has three origins, the applied DC magnetic field, the applied radio frequency (rf) field, and the internal fields.

The applied DC magnetic field, or Zeeman field, sets the spacing of the magnetic energy levels and hence, the precession frequency, through $E = \hbar\gamma H_0$. The temperature, along with the field, determines the total equilibrium magnetization for paramagnetic samples, Curie's law. The applied DC magnetic field defines the z-axis and is denoted by H_0.

A radio frequency field, with frequency chosen equal to the precession frequency, is applied to the spin system to nutate the magnetization or to induce phase coherences between magnetic energy levels. The nutation of the magnetization is the classical picture, and induced transitions, or coherences, are the quantum mechanical picture. The applied rf field is taken to define the laboratory x-axis. In the laboratory frame the rf field is given by

$$\vec{H}_1(t) = 2H_1 \cos\{\omega_{rf}t\}\vec{i}. \qquad (1)$$

The internal fields that arise from other nearby spins, from electrons, and from any other species of spin in the sample will give rise to the distribution of resonance frequencies. Because these internal interactions are dependent on the molecular coordinates (both distance and orientation), they will provide detailed information about the spin environment and the molecular motions. Examples of such interactions are dipole-dipole and anisotropic chemical shift interactions, spin-rotation and indirect nuclear coupling.

The experimentally detected quantities in NMR are the magnitude and the time dependence of the precessing x and y components of magnetization in the laboratory frame.

2.1 CLASSICAL NMR THEORY

Phenomenological equations describing the classical behavior of the magnetization, a macroscopic magnetic dipole in the presence of both static and time-dependent magnetic fields, were written down by Felix Bloch (Blo46) to describe NMR on liquid samples. The NMR Bloch equations (for the case of no relaxation) are

$$\frac{d}{dt} M_i = \gamma(\bar{M} \times \bar{H})_i$$

$$\text{for } i = x, y \text{ and } z \qquad (2)$$

where $\bar{M}_i$ is the component of the magnetization in the i^{th} direction in the laboratory frame, γ is the gyromagnetic ratio of the spins, and H is any applied DC or time dependent magnetic field. To simplify the so-

lution of the Bloch equations, one transforms to a rotating frame with angular velocity Ω about the z axis. The transformed Bloch equations (including relaxation terms) are

$$\frac{d}{dt} M_x = \gamma\left[\bar{M} \times \left(\bar{H} - \frac{\Omega}{\gamma}\bar{k}\right)\right]_x - \frac{M_x}{T_2}$$

$$\frac{d}{dt} M_y = \gamma\left[\bar{M} \times \left(\bar{H} - \frac{\Omega}{\gamma}\bar{k}\right)\right]_y - \frac{M_y}{T_2}$$

$$\frac{d}{dt} M_z = \gamma\left[\bar{M} \times \left(\bar{H} - \frac{\Omega}{\gamma}\bar{k}\right)\right]_z + \frac{M_0 - M_z}{T_1} \qquad (3)$$

where T_1 and T_2 are the relaxation times for the parallel and perpendicular components of the magnetization respectively, and the direction subscripts refer to the rotating frame coordinate system. Results of calculations done in the rotating frame may be transformed back to the laboratory frame by using the rotation matrix

$$\begin{vmatrix} M_x^L \\ M_y^L \\ M_z^L \end{vmatrix} = \begin{vmatrix} \cos(\Omega t + \phi) & -\sin(\Omega t + \phi) & 0 \\ \sin(\Omega t + \phi) & \cos(\Omega t + \phi) & 0 \\ 0 & 0 & 1 \end{vmatrix} \begin{vmatrix} M_x^R \\ M_y^R \\ M_z^R \end{vmatrix} \qquad (4)$$

where the rotating frame x-axis makes an angle ϕ with the laboratory frame x-axis at $t = 0$. Setting $\Omega = \omega_{rf}$, the angular frequency of the rf field, the rf field in the rotating frame becomes time independent and of magnitude H_1. We note that there also is a counter-rotating term due to the rf field in the rotating frame at $-\omega_{rf}$. This term is dropped because it is $2\omega_{rf}$ off-resonance.

To gain an understanding of NMR, one should understand how a signal is produced. Consider the magnetization M_0, in a DC magnetic field H_0, and an rf field H_1, at ω_{rf}, where Ω is the precession frequency γH_0. Defining $h = \gamma H_0 - \omega_{rf}$, the response of M_0 to an rf pulse of duration t_p is described by the Bloch equations. In the rotating frame the components of the magnetization at t_p are

$$M_x(t_p) = (\gamma h/\beta)AQ + M_x(t_i)$$

$$M_y(t_p) = A \sin(\beta t_p + \eta)$$

$$M_z(t_p) = -(\gamma H_1 A/\beta)Q + M_z(t_i)$$

$$Q = \cos(\beta t_p + \eta) - \cos(\beta t_i + \eta)$$

$$\beta = \gamma(h^2 + H_1{}^2)^{1/2} \qquad (5)$$

where A, η, $M_x(t_i)$ and $M_z(t_i)$ are determined from initial conditions and the condition

$$M_z(0)^2 = M_x(t_p)^2 + M_y(t_p)^2\ M_z(t_p)^2,$$

appropriate in the limit T_1, $T_2 \gg t_p$. These equations, for M initially along H_0 and in the limit of $H_1 \gg h$, reduce to the more familiar result for the magnetization $\bar{M}$ immediately after a pulse.

$$M_x(t_p) = 0$$

$$M_y(t_p) = M_0 \sin(\gamma H_1 t_p)$$

$$M_z(t_p) = M_0 \cos(\gamma H_1 t_p), \qquad (6)$$

For times $t > t_p$ (after the pulse, so $H_1 = 0$), the magnetization freely precesses. In the rotating frame the free precession signal is

$$M_x(h,t) = -M_y(t_p) \sin(\gamma h t)$$

$$M_y(h,t) = M_y(t_p) \cos(\gamma h t)$$

$$M_z(h,t) = M_z(t_p). \qquad (7)$$

To accurately reproduce an NMR spectrum, one must consider a distribution of H_o fields. For convenience, choose the distribtution $M(h) = \exp -\{h^2/2\sigma^2\}$, a gaussian of width σ in field units. Then, using equation 6, the total magnetization in the rotating frame for times $t > t_p$ is

$$M_x(t) = \int d(\gamma h)\, M_x(h,t) \exp -\{(\gamma h)^2/2(\gamma\sigma)^2\}$$

$$= 0$$

because of the symmetry of the distribution

$$M_y(t) = \int d(\gamma h)\, M_y(h,t) \exp -\{(\gamma h)^2/2(\gamma\sigma)^2\}$$

$$= M_o \sin(\gamma H_1 t_p) \exp -\{t^2/2\sigma'^2\}$$

$$M_z(t) = M_z(t_p) \quad \sigma'^2 = \sigma^{-2} \qquad (8)$$

Hence even for the case of $T_1 = T_2 = \infty$ (no relaxation), the magnetization in the plane of precession will decay to zero because of the dephasing due to the distribution of off-resonance fields M(h). Transforming back to the laboratory frame and inserting $\gamma H_1 t_p = \pi/2$, the criteria for the shortest pulse that maximizes the amount of magnetization in the plane, the NMR signal is

$$M_z = 0$$

$$M_y = M_0 \exp -\{t^2/2\sigma'^2\} \cos \{\omega_{rf} t + \emptyset\}$$

$$M_x = -M_0 \exp -\{t^2/2\sigma'^2\} \sin \{\omega_{rf} t + \emptyset\} \qquad (9)$$

Hence the NMR signal dies away with a gaussian time dependence because of dephasing.

It is interesting to note that the last step, transforming from the rotating frame into the laboratory frame, has the same effect as heterodyning the rotating frame signal up to ω_{rf}. Calculating the effect on the total magnetization in the rotating frame of the distribution of off resonance fields, M(h), is the same as fourier transforming it with respect to γh, the off-resonance frequency. Since both multiplying and fourier transforming are linear operations the experimentally observed signal, after heterodyning it down to audio frequencies and fourier transforming it with respect to t, will yield $M(\gamma h)$, the distribution of resonance frequencies.

In the approximate calculation above we buried much of the interesting physics when we set $T_1 = T_2 = \infty$, the quantities of real interest in motional studies are just these relaxation times (Noa71). The relaxation times yield information about the molecular motions.

The relaxation time T_2 in liquids is normally obscured by the dephasing. However, an experiment has been designed that will invert the effects of the dephasing due to the distribution M(h), allowing T_2 to be measured experimentally. Hahn showed that applying a second pulse at time τ, after the first pulse, can reverse the effect of dephasing due to an inhomogeneous magnetic field (Hah50). The rephasing of the magnetization causes a signal (an echo) to reappear at 2τ. The echo is essentially two free induction decay (FID) signals back-to-back. The time dependence of the echo amplitude gives a means of measuring T_2. Rephasing techniques are also useful for projecting the NMR signal away from the last pulse, so we can avoid receiver blocking.

Hahn's early work considered both initial and refocusing pulses of equal length. The best refocusing pulse to invert the dephasing due to H_0 inhomogeneity, unlike-spin, and chemical shift interactions is a 180 degree pulse. For dephasing caused by the like-spin, dipolar interaction, the appropriate refocusing pulse is a 90 degree pulse phase shifted 90 degrees from the first pulse.

2.2 SPIN TEMPERATURE

The concept that spins have a temperature (Jee68, Sli80, Abr78, Ram56) that may be distinct from lattice temperature was introduced by Casimer and duPre. Spin temperature has been used by many authors in the discussion of NMR experimental results, single exponential spin-lattice relaxation (Blo48), Hartmann-Hahn cross-polarization (Har62), Waugh's dilute spin signal enhancement pulse sequence (Pin73), the Overhauser effect (Ove53, Ove54, Car53, Car56), and solid state effects such as $T_{1\rho}$, T_{1D} (Loo66, Sli64, Ail71).

To see what it means for a spin system to have a spin temperature, consider the case of N non-interacting spins, I = 1/2. Boltzman statistics for thermal equilibrium give the population of the energy levels as

$$P_+ = N \exp\{\gamma\hbar H/2kT\}$$

for the spins antiparallel to the applied magnetic field H, and

$$P_- = N \exp\{-\gamma\hbar H/2kT\} \tag{10}$$

for the spins parallel to H. Expanding the exponentials and keeping only the first two terms, T_s, the temperature of the spins is related to population difference by

$$T_s = N\gamma\hbar H/(P_+ - P_-) \tag{11}$$

A spin system, if isolated from the lattice, may be at a different temperature. Further more, the spin projections of the spin system may be affected by contact with applied perterbations causing, in

turn, non-equilibrium magnetization. According to statistical mechanics, in thermal equilibrium for $\bar{H} = H_o\bar{k}$ the magnetization for a collection of N independent spins of spin I is given by

$$M_z = \frac{N\gamma\hbar \sum_{-I}^{I} m\, p_m}{\sum_{-I}^{I} p_m} \tag{12}$$

where p_m, the probability that a spin is in its m^{th} energy state, is simply $p_m = (1/N)P_m$. Then in the high temperature approximation ($\gamma H \ll kT$) the sample magnetization is

$$\bar{M} = \frac{N\gamma^2\hbar^2 I(I+1)}{3kT}\bar{H}, \tag{13}$$

which is just Curie's law for paramagnetic samples. Therefore the spin temperature for N spin 1/2 nuclei can be written as

$$T_s = \frac{N\gamma^2\hbar^2\, H}{4kM}, \tag{14}$$

where H is the applied magnetic field and M is the magnetization aligned along H.

In equation 3, the constant M_o was the thermal equilibrium value of the magnetization in H_o. For a collection of N spins of spin

I in thermal equilibrium with the lattice at temperature T, the magnetization is given by equation 13. Then for $h \ll H_0$ (noninteracting spins) and $H_1 = 0$, equation 3 in the laboratory and rotating frames becomes

$$\frac{d}{dt} M_z = \frac{M_0 - M_z}{T_1} ,$$

which yields

$$M_z(t) = M_0 + A \exp -[t/T_1], \qquad (15)$$

where A is to be determined from the initial conditions.

2.3 HAMILTONIANS, RELAXATION TIMES AND LINEWIDTHS

As previously noted, most of the interesting aspects of the physics of NMR are buried in the Bloch equation relaxation times T_1 and T_2, which embody the effects of molecular motion on the spin system (the magnetization). To understand the origins of these relaxation times and the effects of molecular motion on them, we must consider the quantum mechanical description of NMR.

Our studies were on organic molecules composed of carbon, oxygen, and hydrogen. (The words hydrogen and proton will be used interchangably to refer to the proton spin in the hydrogen atom.) To estimate the relative contributions of the different spins to the total hamiltonian, consider the relative number of spins of each kind contained in the sample. This information is displayed in Table I.

TABLE I

Number of Spins in the Samples

	proton	carbon	oxygen
relative number of nuclei/molecule			
glycerol	8	3	3
cyclohexanol	12	6	1
natural abundance of spins	100%	1.1%	.04%
relative number of spins			
glycerol	6,667	25	1
cyclohexanol	30,000	150	1
gyromagnetic ratio x 10^3 $(sG)^{-1}$	260	6.7	3.6

Because of the low natural abundance and small γ of the spin-bearing oxygen, O^{17}, we will completely ignore the presence of the oxygen spins. The spin hamiltonian for an organic sample containing hydrogen (I) and carbon-13 (S) spins, where there are no unpaired electron spins (paramagnetic impurities) is

$$H = H_I^Z + H_S^Z + H_I^{rf} + H_S^{rf} + H_{II}^D + H_{SS}^D + H_{IS}^D + H_S^{CS} \qquad (16)$$

where H^Z is a Zeeman term, H^{rf} is the radio frequency term, H^D is the dipolar term, H^{CS} is the anisotropic chemical shift term.

2.4 PROTON NMR

Because of the lower natural abundance and smaller γ of the carbon spins, compared to protons when doing proton NMR, we will ignore the presence of the carbon-13 spins. Therefore, for proton NMR in organic samples the spin hamiltonian reduces to

$$H = H_I^Z + H_I^{rf} + H_{II}^D. \tag{17}$$

The Zeeman hamiltonian for N protons in a DC magnetic field is given by

$$H_I^Z = -\gamma \hbar H_0 \sum_i I_{zi}. \tag{18}$$

The term in the hamiltonian arising from the interaction of the rf field and the proton spin system, in the laboratory frame is

$$H_I^{rf} = -2\gamma \hbar H_1 \cos\{\omega_{rf} t\} \sum_i I_{xi}, \tag{19}$$

where the rf frequency is $f = \omega/2\pi = \gamma H_0/2\pi$.

The rf pulses are applied to the sample to induce phase coherences between the spin energy levels. (In the classical picture of the Bloch equations the rf pulses nutate the magnetization. In the quantum picture, the phase coherences mean that the time dependence of the expectation values $\langle I_x \rangle$, $\langle I_y \rangle$, and $\langle I_z \rangle$ follow Bloch like equations.) To induce transitions the rf field operator must not commute with the

Zeeman hamiltonian. Hence $\bar{H}_1$ cannot be aligned parallel to H_0, because trivially $[I_z, I_z] = 0$.

The like-spin dipole-dipole term arises from the classical, magnetic interaction between pairs of spins. The form of the dipolar interaction is arrived at by quantizing the well-known classical formula for two interacting magnetic dipoles. Hence, the dipolar hamiltonian for N like-spins, of spin I can be written as (Blo48)

$$H_{II}^{D} = \frac{\gamma^4 \hbar^2}{2} \sum_{i=1}^{N} \sum_{j=1}^{N} \left[\bar{I}_i \cdot \bar{I}_j - 3(\bar{I}_i \cdot \bar{r}_{ij})(\bar{I}_j \cdot \bar{r}_{ij}) \left[\frac{1}{r_{ij}^2}\right] \right] \left[\frac{1}{r_{ij}^3}\right] \qquad (20)$$

where $\bar{r}_{ij}$ is the interspin vector and γ is the spin gyromagnetic ratio.

The dipolar hamiltonian is generally separated in six terms, according to the number of transitions each term will induce. Then we have

$$H_{II}^{D} = 1/2 \sum \sum \{A + B + C + D + E + F\} (\gamma\hbar)^2 (1/r_{ij})^3$$

where

$$A = (1 - 3\cos^2 \theta_{ij})\ I_{iz} I_{jz}$$

$$B = -1/4(1 - 3\cos^2 \theta_{ij})\ (I_i^+ I_j^- + I_j^+ I_i^-),$$

$$C = D^* = -3/2(\sin \theta_{ij} \cos \theta_{ij} \exp i\phi_{ij})(I_{zi} I_j^+ + I_{zj} I_i^-), \text{ and}$$

$$E = F^* = -3/4(\sin^2 \theta_{ij} \exp i2\phi_{ij})\ (I_i^+ I_j^+). \qquad (21)$$

The angles ϕ_{ij} and θ_{ij} are the angles specifying the orientation of $\bar{r}_{ij}$ relative to $\bar{H}_0$. The operators I_i^+ and I_i^- the standard raising and low-

ering operators for spins, $I_j^+ = I_{xj} + iI_{yj} = I_j^{-*}$ (Sch68). The stars denote the complex conjugate.

Since the applied DC magnetic field is large (on the order of 10^4 G) the Zeeman term in the proton hamiltonian will determine the unperturbed energy levels, an assumption we already made when we quantized the spins along H_0. The effect of including the A and B terms in the hamiltonian will be to combine the simple product spin wave functions $|m_1\rangle|m_2\rangle$ -----$|m_N\rangle$ in linear combinations to form eigenstates of the total spin hamiltonian. (For a system of two spins this gives the conventional singlet and triplet states.) The effects of the rest of the dipolar hamiltonian on these new energy levels can be calculated from perturbation theory. The effects (Sli80) will be to:

i) provide a mechanism that allows transitions between nearly degenerate states. In the two spin case this means that transitions are allowed between $|+ -\rangle$ and $|- +\rangle$.

ii) provide a mechanism that allows for transitions between nondegenerate states by admixing small amounts of each state. In the two spin case this means transitions between $|- -\rangle$ and $|- +\rangle$ and, to a lesser extent, between $|+ +\rangle$ and $|- -\rangle$.

By considering the raising and lowering operators one can see that the A and B terms will not induce any changes in the relative number of spin-up to spin-down spins. The A and B terms commute with I_z and so conserve Zeeman spin energy. These terms are responsible for the (nearly) zero frequency transitions and for the distribution of resonance frequencies (the broadening) seen in solid NMR spectra.

The remaining terms (C – F) cause changes in the relative populations of the spin states, and they do not conserve spin energy. These non-energy conserving terms include terms that give rise to transitions at ω_0 ($\Delta E = \hbar\omega_0$), the C and D terms, and terms that induce transitions at $2\omega_0$ ($\Delta E = 2\hbar\omega_0$), the E and F terms. It is the C – F terms that give rise to T_1 and the remainder of T_2 in solids.

2.4.1 Dipolar Broadening of Rigid Lattices

It is well known from elementary quantum mechanics that to induce transitions between energy states at appreciable rates the perturbing hamiltonian must be fluctuating at, or nearly at, a frequency corresponding to that of the transition. In a rigid lattice where all the molecular motions are very slow compared to ω_0 (except for the phonon and libron frequencies, which are too fast to matter,) only 'transitions' of $\Delta E = \hbar\omega \sim 0$ are allowed.

A measure of the linewidth is the second moment of the absorption line. The beauty of describing the NMR lineshape by its moments is that the calculation of the moments does not require that one first solve for the appropriate spin eigenstates (Van48). The second moment of the NMR lineshape is defined in the conventional manner (Sli80, Abr78),

$$M_2 = \frac{\int (\omega - \omega_0)^2 \, f(\omega) \, d\omega}{\int f(\omega) \, d\omega}, \qquad (22)$$

where $f(\omega)$ is the amplitude of the absorption spectrum. (The weak transitions at $\omega = 0$ and $\omega = 2\omega_0$ must be ignored.) The second moment can be calculated from the energy conserving part of the dipolar hamiltonian (Sli80, Abr78). It has been shown that the second moment for N spins, where $\bar{r}_{ij}$ the vector between spins i and j, makes an angle θ_{ij} to Π_0, in the limit of no molecular motion is

$$M_2 = \frac{3}{4N} \gamma^4 \hbar^2 I(I+1) \sum_{i<j}^{NN} \frac{(1 - 3\cos^2 \theta_{ij})^2}{r_{ij}^6} , \qquad (23)$$

where the sum runs over all spins in the sample. For polycrystalline samples that contain randomly oriented crystallites, or samples that are orientationally disordered, M_2 should be averaged over all molecular reorientations, giving

$$M_2 = \frac{3}{5N} \gamma^4 \hbar^2 I(I+1) \sum_{i<j}^{NN} \frac{1}{r_{ij}^6} \qquad (24)$$

in the limit of no molecular motion.

The effect of molecular motion will reduce the apparent size of the second moment. Although the instantaneous value of M_2 is always given by equation 23, the observed second moment is the average of it. To calculate the observed second moment in the presence of rapid motion, average $(1 - 3\cos^2 \theta_{ij})^2$ in equation 23 over the possible values of θ_{ij} allowed by the motion. To calculate the effect of motion on polycrystalline samples, first average over the possible values of θ_{ij} then average over the molecular orientations.

The second moment is often divided into two parts, intramolecular and intermolecular (And53). The separation is made because it takes different motions to completely average each part. Intramolecular second moments are completely averaged to zero by overall molecular rotation. Molecular rotation will also average part of the intermolecular second moment. However, intermolecular second moments are completely averaged to zero, only by rapid molecular diffusion.

The intermolecular second moment due to like spins, for the case of rapid overall molecular rotation but no diffusion, was calculated in a polycrystalline sample by Dimitrieva and Moskalev. For their calculation all the spins were effectively located at the center of their molecule. The lattices considered were fcc, bcc and hcp (Dim64). They showed that for this type of motion the second moment is

$$M_2 = (3/5)\gamma^4\hbar^2 I(I+1)\ c \sum_k (1/r_k)^6 \ , \tag{25}$$

where c is the number of spins of spin I on a molecule. The sum, which runs over the molecular index k, was 115.63 a_0^{-6} for an fcc lattice, 29.05 a_0^{-6} for a bcc lattice, and 14.45 a_0^{-6} for an hcp lattice, where a_0 is the lattice constant. By considering only the interactions of spins on different molecules the complete averaging of the intramolecular interactions was included in the calculation.

Experimentally, in pulse NMR, the second moment is determined from the relationship (Sli80, Abr78),

$$M_2 = \frac{1}{G(0)} \frac{d^2}{dt^2} G(t)\Big|_{t=0}, \tag{26}$$

where G(t) is the FID measured perpendicular to H_1, (M_y following a 90 degree pulse along the x-axis). The need to know the zero time part of the FID is a problem in pulse NMR, because the finite time required for the rf circuits to ring down obscures the early part of the FID. But a variety of techniques have been developed to recover the short time points (Vol78), or to project the signal away from the last pulse while preserving the dipolar interactions (Pin72b, Hah50, Bow82).

2.4.2 Spin Diffusion

The other effect of the secular hamiltonian is to allow for spin diffusion. Spin diffusion arises from the B term, the mutual spin-flip part of the secular hamiltonian. It can be thought of as the spatial diffusion of one spin's orientation at t_0 through the sample via spin flip-flops. In solids these mutual spin-flips are important in understanding the effect of paramagnetic impurities (unpaired electrons) on T_1, which is to drastically shorten it.

Bloembergen explained this effect by postulating that, in a region immediately around the impurity, the spins will quickly relax to thermal equilibrium because of the strong spin lattice coupling due to the large γ of the electrons ($\gamma_e = 2000\gamma_p$). The polarization in this region spreads through the rest of the sample via spin diffusion. This can result in a spin diffusion limited T_1 with a weak temperature dependence.

Spin diffusion is the mechanism that establishes a uniform spin temperature in strongly coupled dipolar spin systems, which will result in purely exponential spin lattice decay curves.

2.4.3 Relaxation Times

In one of the earliest and most important papers on relaxation times, Bloembergen, Pound and Purcell (BPP) (Blo48) gave an excellent derivation of the spin-lattice relaxation time, T_1, and the spin-spin relaxation time, T_2. They considered the case of overall isotropic molecular rotation. As we remarked earlier, the existence of molecular motions will provide randomly fluctuating magnetic fields that give rise to spin polarization along H_0.

2.4.3.1 Spin-Lattice Relaxation Time

For like-spin dipolar coupling (Abr78) the general T_1 relation for a pair of spins of gyromagnetic ratio γ, that are separated by a distance r, is

$$T_1^{-1} = (3/2)\gamma^4\hbar^2 I(I+1)[J^1(\omega_0) + J^2(2\omega_0)] \tag{27}$$

where $\omega_0 = \gamma H_0$ and

$$J^m(n\omega_0) = \int G^m(\tau) \exp -\{in\omega_0\tau\}\, d\tau \tag{28}$$

is the spectral density of the fluctuating internal magnetic fields at $n\omega_0$. The autocorrelation function $G^m(\tau)$ is due to the time dependence of the spacial functions in the dipolar hamiltonian. For random stochastic motion, the analytic form of the autocorrelation function will be a dying exponential. So the autocorrelation function

$$G^m(\tau) = \int F^m(t)\, F^m(t+\tau)\, dt$$

$$= \langle F^m F^m \rangle \exp -|\tau|/\tau_m \tag{29}$$

where τ_m is the correlation time associated with F^m given by

$$F^0 = (1/r^3)(1 - 3\cos^2\theta)$$

$$F^1 = (1/r^3)(\sin\theta \cos\theta \exp -i\phi)$$

$$F^2 = (1/r^3)(\sin^2\theta \exp -i2\phi) \tag{30}$$

In specializing this result to rotational motion, r is considered to be constant. Then the spacial averages become

$$\langle F^0 F^{0*} \rangle = 12/15r^6$$

$$\langle F^1 F^{1*} \rangle = 2/15r^6$$

$$\langle F^2 F^{2*} \rangle = 8/15r^6 \tag{31}$$

Substituting these results into equation 29, where it is assumed that the correlation times are independent of particular spatial functions and equal, $\tau' = \tau_1 = \tau_2$, yields

$$G^1(\tau) = (2/15r^6) \exp -|\tau|/\tau'$$

$$G^2(\tau) = (8/15r^6) \exp -|\tau|/\tau'. \tag{32}$$

Using these results in equation 28 gives the spectral densities as

$$J^1(\omega_o) = (4/15r^6)[\tau/(1 + \omega_o^2\tau^2)]$$

$$J^2(2\omega_o) = (4/15r^6)[4\tau/(1 + \omega_o^2\tau^2)] \tag{33}$$

Finally, substituting the spectral densities into equation 27 and summing over all pairs of spins in the sample gives

$$T_1^{-1} = \frac{2}{3} M_2 \left[\frac{\tau}{1 + \omega_0^2\tau^2} + \frac{4\tau}{1 + 4\omega_0^2\tau^2}\right] \tag{34}$$

where M_2 is the rotationally averagable second moment. The minimum predicted T_1 is $1.05\omega_0/M_2$ when $\tau = 0.616\omega_0$.

If there are two rotational motions (labeled A and B), it can be shown that

$$T_1^{-1} = T_1^{-1}(M_2^A, \tau_A) + T_1^{-1}(M_2^B, \tau_B) \tag{35}$$

where M_2^A is the part of the rotationally averagable second moment modulated by the A motion and M_2^B is the part modulated by the B motion.

For a distribution of motional correlation times, Noack (Noa71) has shown that

$$T_1^{-1} = \frac{2}{3} M_2 \left[\int \frac{\tau D(\tau)\, d\tau}{1 + \omega_0^2\tau^2} + 4\int \frac{\tau D(\tau)\, d\tau}{1 + 4\omega_0^2\tau^2}\right] \tag{36}$$

where the distribution of correlation times $D(\tau)$ is normalized using

$$1 = \int D(\tau)\, d(\ln \tau).$$

2.4.3.2 Spin-Spin Relaxation Time

The spin-spin relaxation time T_2 is derived (Abr78) under essentially the same assumptions used in the calculation of T_1. So for two dipolar coupled spins, where $J^n(n\omega_0)$ is the spectral density at $n\omega_0$,

$$T_2^{-1} = \gamma^4\hbar^2 I(I+1)\{(3/8)J^2(2\omega_0) + (15/4)J^1(\omega_0) + (3/8)J^0(0)\}. \tag{37}$$

Assuming that $\tau_0 = \tau_1 = \tau_2 = \tau$, and the relative motions of the spin pairs are uncorrelated, the result may be extended to include all the spin pairs in the sample. This yields

$$T_2^{-1} = \frac{1}{3} M_2 \left[3\tau + \frac{5\tau}{1 + \omega_0^2\tau^2} + \frac{2\tau}{1 + 4\omega_0^2\tau^2}\right] \tag{38}$$

for a rotational motion modulating a second moment of M_2. The generalization of T_2 to more than one motion or correlation time is the same as in T_1.

2.4.3.3 Rotating Frame Spin-lattice Relaxation Time

In an excellent paper, A. Redfield pointed out that the Bloch equations, which worked in liquids, are inadequate for the complete description of NMR in solid samples (Red55). Experiments by Slichter and Holton (Sli61) showed that the decay of the magnetization, when aligned parallel to H_1, is more like T_1 than T_2. This experiment measures the spin-lattice relaxation time in the rotating frame, $T_{1\rho}$, parallel to the rotating rf field. The Bloch equations when applied to the

experiment where the magnetization is aligned parallel to H_1 in the rotating frame, predict a decay time of T_2.

Appropriate calculations of $T_{1\rho}$ have been done by several authors. Chihara (Sod74) calculated $T_{1\rho}$ by transforming the spin hamiltonian, equation 17, into the rotating frame using the unitary operator $U = \exp -\{i\omega I_z t\}$. For overall rotational motion of two dipolar-coupled spins

$$T_{1\rho}^{-1} = \frac{3}{8} \gamma^4 \hbar^2 I(I+1) \{J^0(2\omega_1) + 10J^1(\omega_0) + J^2(2\omega_0)\} \tag{39}$$

in the weak collision limit ($\tau << T_2^{RL}$), and for $H_1 > H_L$ the local field. The local field $H_L = [(1/3)M_2]^{1/2}$ (Sli61), and where $\omega_1 = \gamma H_1$, assuming a single exponential rotational correlation function. Summing over all the spins gives $T_{1\rho}$ in terms of the rotational correlation time τ and the rotationally averagable second moment. The result is

$$T_{1\rho}^{-1} = \frac{1}{3} M_2 \left[\frac{3\tau}{1 + 4\omega_1^2\tau^2} + \frac{5\tau}{1 + \omega_0^2\tau^2} + \frac{4\tau}{1 + 4\omega_0^2\tau^2}\right] \tag{40}$$

This predicts a minimum at $T_{1\rho} = 4.0\omega_1/M_2$ when $\tau = 0.5\omega_1$. The inclusion of two motions and distributions of rotational correlation times is the same as was done for T_1.

2.4.3.4 Dipolar Field Spin-lattice Relaxation Time

There is one other spin-lattice relaxation time that is typically measured, the spin-lattice relaxation in the internal fields,

T_{1D}. Measurements of T_{1D} were made by turning down the applied field (Abr58, Str64) or by removing the sample from the magnetic field (Jon67). Others showed that T_{1D} can be measured in the rotating frame without removing the sample from the Zeeman field (Sli61, And62, Ste73). Jeener showed that a simple three pulse sequence can be used to measure T_{1D} in the Zeeman field (Jee67). In the slow motion limit, $\tau > T_2^{RL}$ for rotational motion

$$T_{1D} = (1 - p)^{-1}\tau \tag{41}$$

where p is the probability that after one jump the local fields will be unchanged.

2.5 CARBON-13 NMR

Recall from Table 1 that carbon-13 is a 1.1% naturally occuring isotope. Since protons are 100% spin bearing, the proton spins must be included in the hamiltonian for carbon spins. The spin hamiltonian for carbon-13 NMR experiments is

$$H = H_I^Z + H_S^Z + H_I^{rf} + H_S^{rf} + H_{II}^D + H_{IS}^D + H_S^{CS} + H_{SS}^D. \tag{42}$$

The first five terms are the familiar Zeeman (equation 18), rf (equation 19) and dipolar (equation 20) terms, with appropriate substitutions for the S spins. The last term, H_{SS}^D, is superficially like H_{II}^D, but it will be argued later that this is not the case because of the presence of the anisotropic chemical shift term, H_S^{CS} and H_{IS}^D. (With hindsight the last four terms in equation 42 have been listed in descending order of their size.)

2.5.1 Unlike-spin Hamiltonian

The unlike-spin hamiltonian, H_{IS}^{D}, arising from the interaction between N_I spins of spin I and M_S spins of spin S, is

$$H_{IS}^{D} = \gamma_I \gamma_S \hbar^2 \sum_{i=1}^{N} \sum_{s=1}^{M} \left[\frac{1}{r_{is}^3}\right]\left[\bar{I}_i \cdot \bar{S}_s - \frac{3(\bar{I}_i \cdot \bar{r}_{is})(\bar{S}_s \cdot \bar{r}_{is})}{r_{is}^2}\right], \tag{43}$$

where the applied DC magnetic field defines the z-axis and $\bar{r}_{is}$ is the interspin vector, between the i^{th} I spin and the s^{th} S spin. The unlike-spin hamiltonian can be separated by a similar procedure as used for like-spins, giving

$$H_{IS}^{D} = \gamma_I \gamma_S \hbar^2 \sum_{i=1}^{N} \sum_{j=1}^{M} \left[\frac{1}{r_{is}^3}\right]\{A + B + C + D + E + F\}.$$

The terms A - F are denoted as

$$A = (1 - 3\cos^2 \theta_{is}) I_z S_{zs},$$

$$B = -1/4(1 - 3\cos^2 \theta_{is})(I_i^+ S_s^- + S_s^+ I_i^-),$$

$$C = D^* = -3/2 \sin \theta_{is} \cos \theta_{is} \exp (i \phi_{is}) (I_{zi} S_s^+ + S_{zs} I_i^+),$$

$$E = F^* = -3/4 \sin^2 \theta_{is} \exp (i2\phi_{is}) (I_i^+ S_s^+), \tag{44}$$

where $I^{\pm}$, $S^{\pm}$ are the conventional raising and lowering operators and the star denotes the complex conjugate. Only the A term commutes with the carbon Zeeman hamiltonian and therefore is secular. The other terms all do not conserve energy and are non-secular. The second moment arising from the dipolar interactions for S spins (carbon) in the presence of I spins (proton) due to the secular part of the dipolar hamiltonian is

$$M_2 = \frac{3}{4}\gamma_S^4\hbar^2 S(S+1)\,\frac{1}{M}\sum_{\substack{i=1\\ j=1}}^{M}\frac{(1-3\cos^2\theta_{ij})^2}{r_{ij}^6} + \frac{1}{3}\gamma_I^2\gamma_S^2\hbar^2 I(I+1)\,\frac{1}{N}\sum_{i=1}^{M}\sum_{s=1}^{N}\frac{(1-3\cos^2\theta_{is})^2}{r_{is}^6} \qquad (45)$$

2.5.2 Anisotropic Chemical Shift

The chemical shift in molecular solids arises from the response of the electrons to the applied field H_o. The presence of H_o induces small net currents in the bonding electrons. The induced currents, in turn, create magnetic fields at the spin sites and the magnitude and direction of the fields at the nuclei will depend on the position of the nucleus relative to the currents path.

The calculation of frequency shifts in the high field limit is formally treated by Slichter (Sli80), Abragam (Abr78), Ramsey (Ram56), Bloembergen and Rowland (Blo53), and others (Die6). Ramsey wrote down a formal solution for the induced magnetic field at a nucleus,

$$\bar{H}_s = \frac{1}{c}\sum_j\int\frac{\bar{r}_j \times \bar{J}_{oj}(\bar{r}_j)}{\bar{r}_j^3}\,d\tau_j \qquad (46)$$

where the sum runs over the electrons. The induced current due to the j^{th} electron is given by

$$\bar{J}_{oj}(\bar{r}_j) = -\int\left[\frac{\hbar e}{2mi}\psi^*\nabla_j\psi - \psi\nabla_j\psi^* - \frac{e}{mc}\bar{A}_{oj}\psi^*\psi\right]d\bar{\tau}',$$

$$d\bar{\tau}' = d\tau_1 \ldots d\tau_{j-1}\, d\tau_{j+1} \ldots d\tau_N \tag{47}$$

where Ψ is the N electron wave function in the presence of H_0, and $\bar{A} = (1/2)\Pi_0 \times (\bar{r}_j - \bar{R})$.

For organic molecules, even small ones like glycerol, this calculation can be a formidable task, but several facts emerge from the theory. The chemical shift is linear in H_0, it will depend on the molecular orientation with respect to H_0, and for a solid that is orientationally disordered, the observed spectrum will be weighted according to the probability distribution of molecular orientations. Using a model that assumes uniaxial symmetry and $\sigma_\perp > \sigma_\parallel$, Bloembergen and Rowland calculated spectrum shown in Fig. 1. The angular dependence of the anisotropic chemical shift, relative to the isotropic (liquid) resonance frequency ω_0, is

$$\omega(\theta) - \omega_0 = \omega_0 \Delta\sigma \, (\cos^2 \theta - \{1/3\}), \tag{48}$$

where θ is the angle between the molecular axis and H_0, and $\Delta\sigma$ is the chemical shift anisotropy $\sigma_\parallel - \sigma_\perp$. Experimentally $\omega_0\Delta\sigma/2\pi$, the chemical shift linewidth for glycerol, is found to be ~ 1 KHz at $\omega_0/2\pi$ = 20.8 MHz. By way of comparision, the inhomogeneous dipolar linewidth from the carbon-carbon interaction is found to be ~ 70Hz after removing the broadening due to the carbon-proton dipolar interaction (Kuh82).

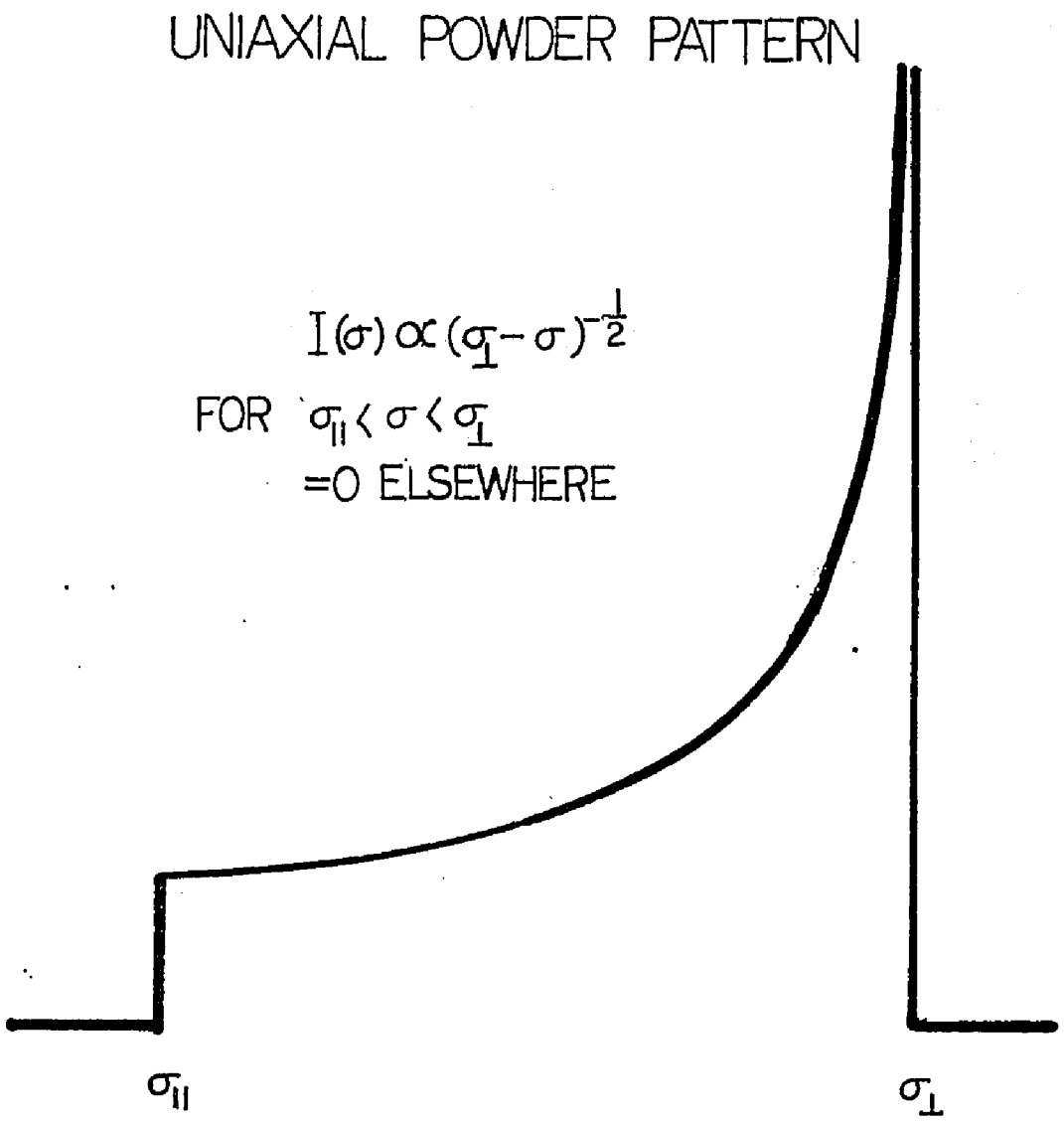

Figure 1: Powder pattern for an axially symmetric chemical shift tensor with $\sigma_{11} < \sigma_\perp$. The orientation and frequency are connected through equation 48.

2.5.3 Carbon Linewidth in the Rigid Lattice

Now we are in a position to evaluate the second moment of the carbons. The existence of the chemical shift will lift the degeneracy of the carbon spin states so it is appropriate to consider them as semi-like spins (Van79). The result of this is to make terms like $S_i^+ S_j^-$ non-energy conserving. Hence the secular hamiltonian of the carbon spins is

$$H = \frac{\gamma_I \gamma_S \hbar^2}{2} \sum_{\substack{i=1 \\ s=1}}^{NM} \frac{1}{r_{is}^3} (1 - 3\cos^2\theta_{is})\, I_{zi} S_{zs}$$

$$+ \frac{\gamma_S^2 \hbar^2}{2} \sum_{\substack{i=1 \\ j=1}}^{MM} \frac{1}{r_{ij}^3} (1 - 3\cos^2\theta_{ij})\, S_{zi} S_{zj}$$

$$+ \gamma_S \hbar H_0 \sum_{i=1}^{M} \sigma_i(\theta,\phi)\, S_{zi}$$

$$- \gamma_I \hbar H_0 \sum_{i=1}^{N} I_{zi} - \gamma_S \hbar H_0 \sum_{i=1}^{M} S_{zi} \qquad (49)$$

The observed second moment, using the result from equation 45, and denoting it an M_2' gives

$$M_2 = M_2' + \frac{5}{2} \gamma_S^2 \frac{H_0^2}{M} \sum_{i=1}^{M} \sigma_i^2 \qquad (50)$$

However this is not the whole story. It has been shown that the proton-carbon dipolar hamiltonian can be forced to zero by an intense rf irradiation at ω_I(Pin70). The effect of this irradiation is to induce rapid I spin flips averaging I_{zi}, the z-component of the proton spins, to zero. This leaves only the carbon-carbon and anisotropic chemical shift interactions contributing to the carbon-13 linewidth. These two terms are fundamentally different, as can be seen by considering the effect of a 180 degree pulse on the secular hamiltonians. Since the dipole-dipole term is bilinear in S_z, a 180 degree pulse will invert both spins, leaving the hamiltonian unchanged. However the chemical shift term is linear in S_z, so a 180 degree carbon pulse will invert the spin projection, which will change the sign of the hamiltonian. The invertible hamiltonians give rise to 'inhomogeneous' linewidths. (Inhomogenous linewidths were first seen as resulting from inhomogenous magnetic fields.)(Blo48) The non-invertible hamiltonians (by contrast) give rise to homogeneous linewidths. The anisotropic chemical shift contribution to the second moment (in glycerol) is much larger than the carbon like-spin contribution to the second moment. Such an inhomogeneously broadened line may be considered to be composed of a group of homogeneous lines (isochromates) that are shifted in frequency relative to each other by the inhomogeneous interaction. These inhomogeneous frequency shifts (in glycerol) are due to anisotropic chemical shifts. Consequently the observed second moment or the linewidth in glycerol under vigorous proton spin stirring is due to anisotropic chemical shift.

2.5.4 Carbon Spin-Lattice Relaxation

The spin-lattice relaxation time for the carbon spins is due to three interactions. In organic samples that have large anisotropic chemical shifts, they are: the IS dipole interaction, the anisotropic $\sigma H_0 S$ chemical shift interaction, and the SS dipole interaction. In samples where the molecular motions are slow, these interactions will result in a long carbon T_1.

Chapter III

SPECTROMETER

The spectrometer used in these experiments was a homebuilt, high-power, computer controlled, pulse spectrometer, with two phase detection.

3.1 MAGNETS

Two magnets were used, a low impedance Varian V-3900 and a high impedance Varian V-4012HR. Both are iron-core magnets.

3.1.1 Low Impedance Magnet

The low impedance magnet has a maximum field of 20 KG, a gap of 3.5 cm, and tapered pole caps. The H_0 inhomogenity is corrected using shim coils. The current, 200 amps maximum at 60 volts, is controlled by 59 pass transistors in parallel. The field regulation for the glycerol experiments used a Hall probe, which was original equipment, and an external NMR field-frequency locker, which will be discussed in detail later. For the cyclohexanol experiments the field stability controls were modified to be a combination of current regulation, flux locking (for short term stability) and NMR field-frequency locking (for long term stability). The current regulator controls the bank of 59 pass transistors by measuring the voltage across a 1/3 ohm resistor in series with each emitter. The resulting voltages are summed (averaged) and the

result is compared to a reference voltage, generated by a battery and a voltage divider network. The difference, or error, is amplified and fed back to the pass transistor bank in place of the error signal from the Hall probe.

3.1.2 High Impedance Magnet

The high impedance magnet has a gap of 4.5 cm. Its maximum field is 15 KG for the maximum current, 2 amps at 2.5 KV. The power supply uses a variac for course voltage control and a bank of 8 pass tubes in parallel as a series regulator. The commercially installed equipment included current regulation and flux locking. We added the external NMR field-frequency locker to increase long term stability of the magnetic field.

3.2 LOW IMPEDANCE FLUX LOCKER

The flux locker consists of two pairs of Hemholtz coils wound coaxially and placed around the pale faces of the magnet. One pair of the coils called the pickup coils (2000 turns), is used to detect the fluctuations of the magnetic field. The detected signal is then amplified, and time integrated. The amplified signal is fed back to the second pair of coils, the buckout coils (500 turns), in a negative feedback arrangement. The time integrated signal is sent to the magnet power supply to be fed into the existing feedback circuit. The feedback to the magnet power supply reduces the long time burden on the bucout coils.

3.3 NMR FIELD-FREQUENCY LOCKER

The reason one cannot rely only on flux-locking circuits to stabilize the field is that slow drifts of the DC field will induce voltages that are below the amplifier noise, and so will be ignored. Viewed another way, amplifier drifts and noise produce slow field drifts. Our solution was to use an external NMR locker to follow these slow drifts. The NMR lock sample is F^{19} in C_6F_6, a liquid at room temperatures. It is heavily doped with DPPH and TEMPO, both stable free radicals (inpaired electrons). Enough DPPH and TEMPO was added so that T_1 was reduced to ~ 20 milliseconds. The NMR locker signal is produced by irradiating the sample with a continuous series of pulses of amplitude H_1 and length t, spaced at intervals of τ. The steady state response of the magnetization to these pulses is the same as it would be to constant irradation with a lower rf field, H_i' given by,

$$H_1' = H_1\frac{t}{\tau}. \tag{51}$$

Since the sample is a liquid, the steady state response is predicted by the Bloch equations. In the rotating frame the magnetization is

$$\begin{aligned} M_x &= \gamma^2 h H_1' T_2^2 C M_0 \\ M_y &= \gamma H_1' T_2 C M_0 \\ M_z &= [1 + (\gamma h T_2)^2] C M_0 \end{aligned} \tag{52}$$

where

$C = \{1+(\gamma h T_2)^2 + (\gamma H_1')^2 T_1 T_2\}^{-1}$ and $h = H_0 + \omega_{rf}/\gamma$.

The phase of the rf pulses is alternated by 180 degrees every other rf pulse. This produces a fourier spectrum with components at $f = n/\tau$, n odd. The carrier at f_0 and the even sidebands (the components with even values of n) are supressed by the phase alternation scheme. The magnetic field is adjusted so that $\gamma_F H_0 = f_0 - f$, or the spins are driven by the first lower sideband. Since the pulse spacing τ determines f, the driving frequency of the spins can be adjusted by varying τ or f_0, the basic rf frequency. A liquid sample is used so the width of the NMR line (Δf) is less than 2f, the sideband spacings. Hence the spins respond only to one sideband.

The receiver is gated on only between pulses and detects the spins response at $f_0 - f$. The condition $\Delta f \ll f$ says that the spin system will 'ring' for much longer than the time between pulses. So this is a 'continuous wave' experiment.

Phase sensitive detecting the receiver output M(t) against f_0 gives a beat note at f. Hence the audio signal (f) has a period equal to 2τ the time between the $\phi = 0$ (or $\phi = 180$) degree transmitter pulses.

Phase sensitive detecting the audio signal by phase inverting it during every other half cycle yields a signal that, when time-averaged, will yield zero for exact resonance, $\gamma H_0 = f_0 - f$. When the spins are off-resonance their response will be phase-shifted because of dispersion, making the time average of the phase detected audio signal non-zero. The sign and magnitude of the time-averaged signal will tell

how far and in which direction the field has moved. The voltage corresponding to the time-averaged signalis sent to the flux stabilizer, then on to the magnet power supply.

To prevent drifts of the rf frequency used in the locker relative to the main synthesizer, the rf is injection locked to the main synthesizer's 1 or 5 MHz output.

3.4 SHIM COILS

We mentioned earlier that the 20 KG, DC magnetic field was inhomogeneous, an experimental detail that we have been ignoring. The inhomogeneity would normally give rise to broading of the NMR lineshape. But the shim coils are used to produce gradients that oppose the gradients due to the inhomogenity of H_0. The shim coils are used to correct for field inhomogenities up to second order. The homogeneity requirements are most severe in the glycerol experiments that used spectral hole-burning. These experiments required that ΔH_0, the variation in H_0 over the sample volume, must satisfy $\gamma\Delta H_0 << \Delta\omega^{CS}_{RL}$, the distribution resonance frequencies due to anisotropic chemical shift.

3.5 THE RF: FREQUENCY GENERATION AND TRANSMITTERS

The main rf sections of the spectrometer use two or three frequencies, depending on the experiment. Two frequencies are used for single resonance experiments and three frequencies for double resonance experiments. The frequencies are generated by a General Radio synthesizer and by a crystal-controlled oscillator. The synthesizer generates

the 1 or 5 MHz signal used by the NMR field-frequency lock, the 30 MHz used as the intermediate frequency (IF), and f_0 + 30 MHz used as the main frequency. For double resonance experiments the proton frequency is generated by the crystal controlled oscillator (41.46 MHz), so that the synthesizer can be used for the carbon frequency. Block diagrams for the rf circuits for both single and double resonance experiments are shown in Figs. 2 and 3.

The spectrometer is a four-phase pulse spectrometer. The rf phasing and gating is done at 30 MHz. This is then hetrodyned in a single sideband transmitter against f_0 + 30 MHz. The resulting phased and gated rf, at f_0, is amplified by power transmitters. A class A, 300 watt continuous duty cycle, is used for frequencies less than 30 MHz. A two-stage, tuned, class C tube amplifier (using 4CX series tetrodes) with a 10 watt broadband amplifier is used for the double resonance proton frequency, f_0 = 83 MHz. The DC power supplies for the 3E29 used in the first stage, have upper limits of 250V on the screens and 800V on the plates. The 4CX250s used in the output stage has limits of 500 V on the screens and 2 KV on the plates.

The rf pulse lengths are set using one-shot pulsers built around 555 and 74121 timing chips. Waiting intervals or pulse lengths that are varied during a single experiment, for example the spin locking pulse in $T_{1\rho}$ experiments, are controlled by timing programs in the Apple II microcomputer.

The rf pulse amplitude in one experiment (spectral hole burning) must be changed during the course of a single pulse sequence. This is achieved by placing a current-controlled attenuator (a double-bal-

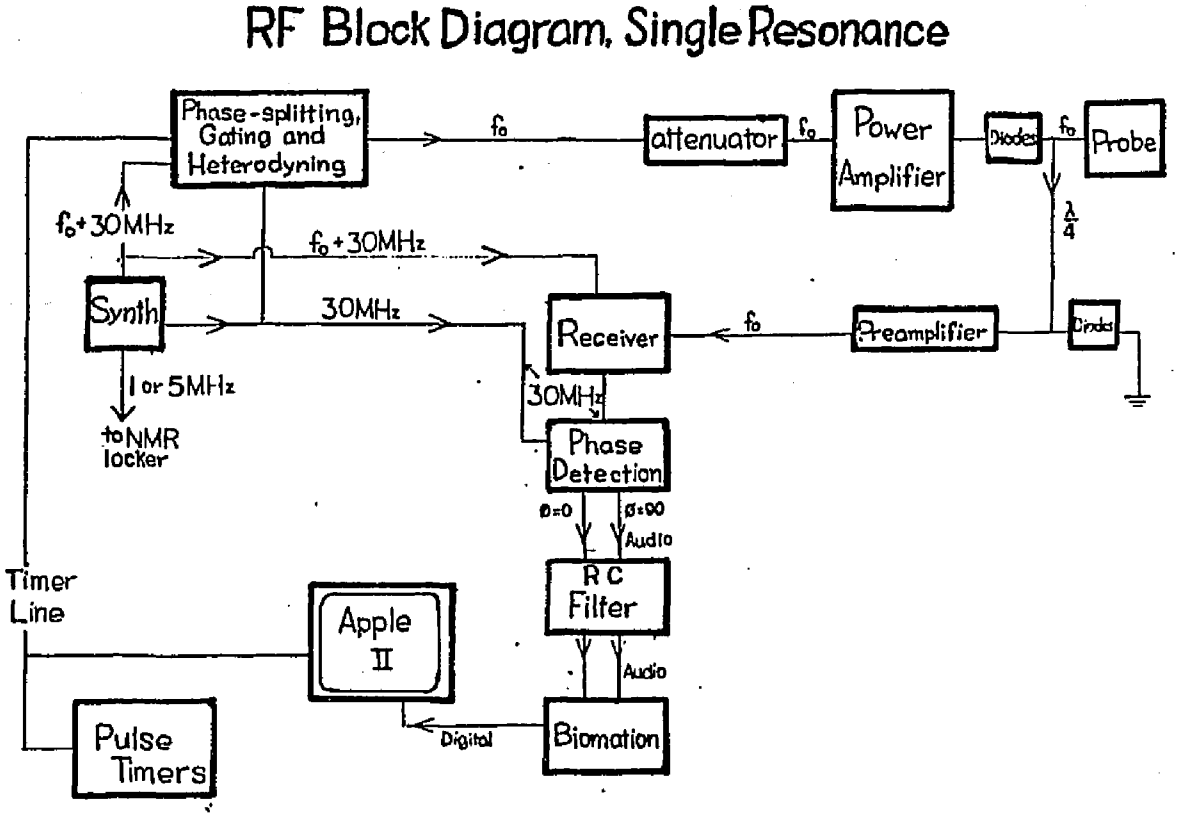

Figure 2: Block diagram of the spectrometer used in the single frequency experiments.

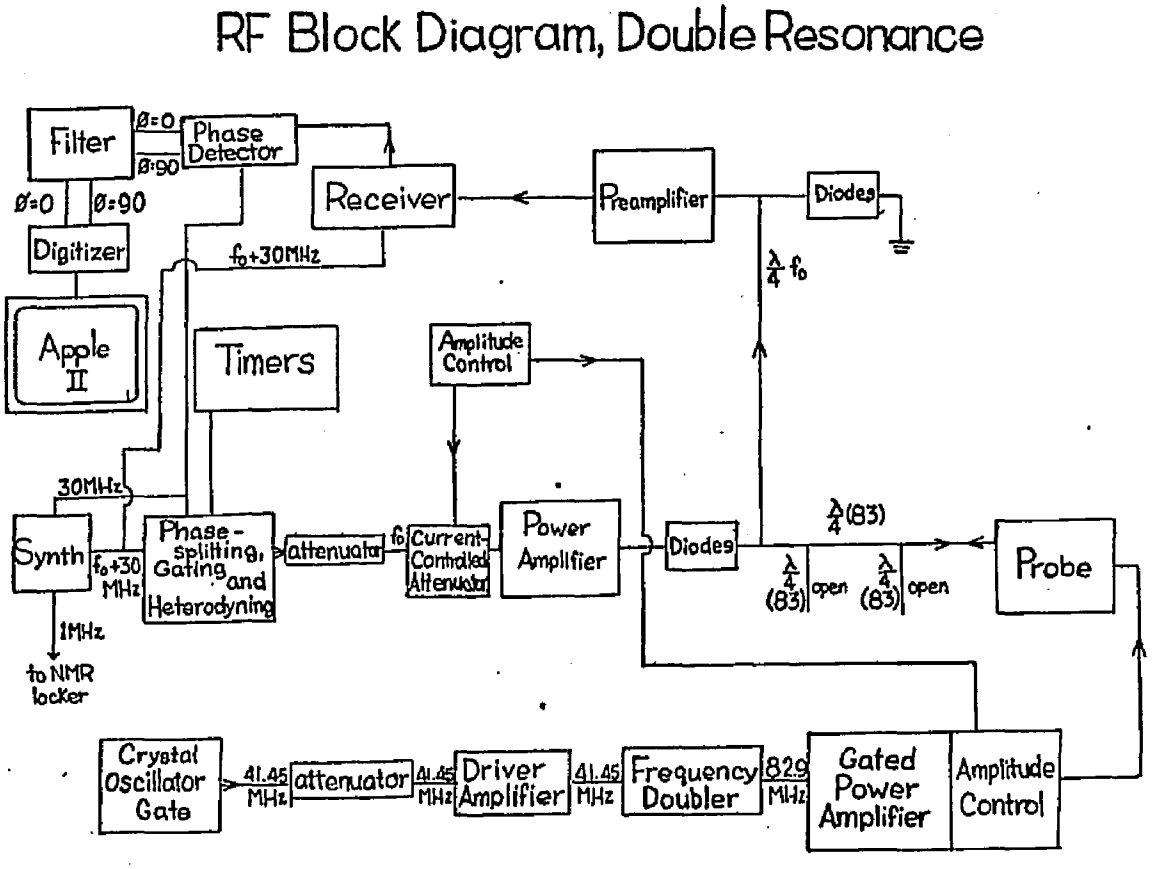

Figure 3: Block diagram of the spectrometer used in the double resonance (protons and carbons) experiments.

anced mixer) in front of the class A amplifier, or by controlling the DC screen voltage on the 4CX250 final stage.

A single coaxial cable is used to connect the probe to the rf transmitters and preamplifiers. To isolate the different rf components (i.e., the receiver during transmit, or the transmitter during receive), we used passive switching (crossed diodes) and quarter wave tranformers (Fuk81). Quarter wave cables have the property that the input impedance $Z_{IN} = Z_0^2/Z_T$ where Z_0 is the characteristic cable impedance and Z_T is the terminating impedance.

3.6 PROBES

The basic circuit used in NMR probes is the LC tank circuit. The input impedance of a parallel tank circuit is high, typically 1000 ohms. The transmitters have 50 ohm output impedances and the preamplifiers have 50 ohm input impedances. So impedance matching schemes are needed. One such scheme is to use capacitive coupling (Kan80, Cro76). For double resonance we used two such circuits back to back. The other impedance matching scheme we used was transformer coupling of the transmitter and the LC tank circuit. This circuit, which had different transmit and receive lines, used a high input impedance preamp. This circuit also had a Q-switch.

The Q, or quality, of a tuned circuit is defined as the number of radians required for the power (the square of the voltage) to decay to 1/e of its initial value. Q is given by $\omega L/r = 1/\omega Cr$, where ω is $2\pi f$, f is the characteristic frequency of the LC circuit, and r is the series ohmic resistance of the circuit. Circuits of high Q have

narrow band widths, which helps in achieving high H_1. But high Q circuits require long times to ring down after an rf pulse to levels such that the NMR signal is observable. A method to reduce this ring down time, which is quite long at low frequencies, is to switch an additional resistive element into the LC circuit during ring down (Can77). This is the principle of the Q-switch.

3.7 PREAMPLIFIERS

We used two types of preamplifiers in these experiments, 50 ohm input impedance preamplifiers and a high (~ 1000 ohm) input impedance preamplifier. Preamplifiers are low noise, high gain amplifiers, which operate at f_o. Since preamps, even with the protection provided by the passive switching, are subjected to 1 volt pulses during transmit they must be able to recover quickly from saturation. We used four different preamps in these experiments, a commercial preamp with 30 decibel gain that recovered slowly from saturation, two homebuilt, tuned preamps with ~ 30 decibel gain that operate at 83 MHz and 21 MHz and one homebuilt, wide band, high impedance preamp. The homebuilt preamps did not have excessive recovery problems.

3.8 RECEIVER BLOCKING

In all pulse NMR experiments the early part of the FID is obscured by the rf pulse, by the ringing down of the LC tank circuit from the pulse, and by the recovery of the preamp from saturation. All of these effects are lumped together and called receiver blocking (Fuk81). The receiver blocking cannot be eliminated, but its effects can be mini-

mized by Q-switching (active switching), diode protection (passive switching) and the use of fast recovery preamps.

Receiver blocking creates problems in data reduction. Such as in determining the second moment using equation 26 (which requires knowledge of the FID at zero time) and in fourier transform NMR where the zero time signal (the 0^{th} moment) determines the area under the absorption spectrum in the fourier transform. The higher moments are also important because they determine the shape of the absorption curve.

3.9 RECEIVER

The receiver used in these experiments is a gated, superheterodyne (30 MHz IF), variable gain amplifier with in-phase and quadrature phase detection. The amplification and phase detection is done at 30 MHz. The output is at audio frequencies in two quadrature phase,

The audio signal is smoothed by an RC filter to reduce the high frequency noise and eliminate any 30 MHz leakage. The RC filter has variable time constants, with either 6 or 12 decibels per octave rolloff.

3.10 DIGITIZER AND SIGNAL STORAGE

The two phases of the audio frequency signal are digitzed by a Biomation 2805A, transient digitizer with a variable time base (0.2μs/pt to 50μs/pt). The Biomation digitizes 2048 points of data per channel, of which 1024 points are transferred to the Apple II microcomputer for signal averaging (accumulative addition) and data storage.

3.11 COMPUTER

The Apple microcomputer is used for signal averaging and storage, data reduction, and fourier transforming. The computer also is used for timing some parts of the pulse sequences. The language used is First, a compiled microcomputer language developed for laboratory use in Apple computers. If a permanent record of the data, for either time or frequency domain is desired, it is stored on diskettes.

3.12 TEMPERATURE CONTROL

The temperature regulators used in these experiments were variable temperature gas flowing systems that used N_2 or He gas. Nitrogen was used in the glycerol experiments and in the cyclohexanol experiments above 110 K. The cyclohexanol experiments below 110 K used He. The temperature controllers were an on-off heater for N_2 and a proportional heater for He. Both temperature controllers used 100 ohm (nominal resistance at R.T.) platinum resistance thermometers.

Chapter IV

THE GLYCEROL EXPERIMENT

4.1 BACKGROUND

Glycerol ($CH_2OH - CHOH - CH_2OH$) is an organic material that forms a viscous liquid at room temperature. The high viscosity is due to the hydrogen bonding that occurs between the OH groups on neighboring molecules. As the temperature is lowered the mean number of OH groups involved in hydrogen bonding increases. This results in the viscosity steadily increasing as an increasing number of molecules are being included in the randomly oriented molecular 'chains.' When the temperature is lowered to 185 K, glycerol undergoes a 'transition' to a translationally and orientationally disordered glass (Gib23). In other words, at and below T_g the molecules are locked into a liquid-like metastable structure that will not readily transform into the prefered crystalline phases (Gib23, Par27).

The correspondence between viscous liquids and glass formation has been known for a long time. Park and Huffman (Par27), in a paper that was one of the first systematic calorimetric studies of glassing materials, studied the glass transition in several organic materials that differed in the number of OH groups per molecule. They showed that as the number of OH groups per molecule increased, so did the glass transition temperature.

The transition from the liquid to the glass is a kinetic phenomenon. It is seen as a step-like change in the specific heat over a small (~ 5 K) temperature range. In glycerol the specific heat drops 55% near 185 K, the glass transition temperature (Gib23, Par 27).

As stated in the introduction, glycerol forms a 'liquid' glass that is both translationally and orientationally disordered. These terms, translational and orientational disorder can be defined as follows. Define a function $F(\bar{r})$ by replacing all the molecules in the sample with delta spikes at their centers of mass:

$$F(\bar{r}) = \sum_{k} \delta(\bar{r} - \bar{r}_j), \tag{53}$$

where $\bar{r}_j$ is the location of the center of mass of the j^{th} molecule. Fourier transform the functions $F(\bar{r})$ to get $K(\bar{k})$ where

$$K(\bar{k}) = \int d\bar{r}\, F(\bar{r}) \exp i\bar{k}\,\bar{r} \quad . \tag{54}$$

If the spectrum K has delta spikes at discrete values of $\bar{k}$, then the sample is translationally ordered. However if K does not show a discrete nature, the sample is disordered. In general, K will contain both delta spikes at discrete values of K and a continous background. The complete absence of delta spikes means the sample is translationally disordered.

For the case of orientational disorder a loose defination is, if the knowledge of the i^{th} molecule's orientation can be used to predict the orientation of another molecule at distance r away, in the limit of r approaches ∞, then the sample is orientationally ordered.

However if no such scheme is possible then the sample has orientational long-range order.

Because glassy glycerol is disordered at zero kelvin, it has a residual entropy of 23.5 J/mole-K (Gib23). The measurement of the residual entropy of glycerol is a fairly difficult measurement because of glycerol's near refusal to crystallize. However, the ease with which the disordered state can be achieved has led to a substantial number of studies on glycerol: calorimetric (Gib23, Par27), dielectric (Mor34, Dav51, McD62, Mcd63, Lit63, Dem73), acoustic (Rie57), optical scattering (Dem74, Pin68), and NMR (Wol79, Noa67) under a wide range of temperatures and pressures.

We studied molecular reorientations in glycerol just above the glass transition. The glass transition is kinetic in nature and an understanding of the motions near the glass transition is essential to understanding it. The technique used in this work is spectral hole-burning which exploits the existence of the anisotropic chemical shift to tag and follow the molecular reorientations.

4.2 EXPERIMENTAL

The sample used in these experiments was Aldrich gold label glycerol. A small amount of ferric chloride was added to reduce T_1 of the protons in the glass to a reasonable value of ~ 5 s. The 1.5 gram sample was held in a 13 mm OD test tube that was kept stoppered at all times. The sample temperature was measured with a thermocouple in a thinwall glass tube (thermocouple well) that dipped into the sample.

All of the data reported here were taken on freshly cooled samples. The sample was warmed to room temperature after at most six hours at low temperatures before continuing the experiment. The samples were always clear with almost no cracks and the data was reproducible. In our preliminary work we obtained irreproducible results on a sample kept cold for two weeks. This sample had many cracks, possibly due to crystallization But more likely due to absorption of atmospheric water.

4.3 PULSE SEQUENCE

The pulse sequence used in these experiments is shown inFig. 4. The first part of the pulse sequence uses the part of the rotating frame IS dipolar hamiltonian to dynamically polarize the carbon spin system (McC67, Pin72b, Har62, Meh76).

4.3.1 Cross Polarization

Consider a fully relaxed proton spin system in a field H_0 at a lattice temperature T_L. A 90-degree pulse is applied to the protons, after which the rf is phase-shifted 90 degrees so H_{1p}, the proton rf magnetic field, lies parallel to the nutating proton magnetization. Then, in the rotating frame, the proton spin system has a spin temperature of

$$T_p^{rf} = C_I H_{1p}/M = H_{1p}T_L/H_0 . \qquad (55)$$

where $C_I = (\gamma_I \hbar)^2 I(I+1)N_I/3k$.

During the spin-locking of the protons, a carbon pulse H_{1c} is turned on. The amplitudes of the two rotating frame magnetic fields are relat-

ed by $H_{1c} = (\gamma_p/\gamma_c)\, H_{1p}$. Then the spin systems can exchange energy via the transformed IS dipolar hamiltonian $I_{zi}S_{zs}$, (x is the direction of H_1 in each of the rotating frames). So the two spin systems will come to the same spin temperature T_s^{rf}. This final temperature will be approximately equal to T_p^{rf}, the protons spin temperature, because the number of protons is much greater than the number of carbons and $\gamma_p \sim 4\gamma_c$. After the two spin systems have come to an equilibrium, the rotating frame carbon spin temperature is

$$T_c^{rf} = (H_{1p}/H_0)T_L. \tag{56}$$

Then both cross polarization rf pulses are turned off and a phase-shifted, 90 degree pulse is applied to the carbon spin system to store the carbon magnetization along H_0. The carbon magnetization following the cross-polarization is given by

$$M_C = C_S\, H_{1c}/T_c^{rf}$$

where $C_S = (\gamma_s \hbar)^2 S(S+1)N_S/3k$

Therefore, $M_C = C_S H_0 T_L (H_{1c}/H_{1p})$

$$= M_{eq\ C}\ (\gamma_p/\gamma_c)$$

$$\sim 4M_{eq\ C}\ , \tag{57}$$

where $M_{eq\ C}$ is the thermal equilibrium carbon magnetization. So the carbon magnetization is approximately four times its thermal equilibrium value.

The two beneficial effects of cross-polarization are that the carbons can be polarized in a time T_1 of the protons, which is often

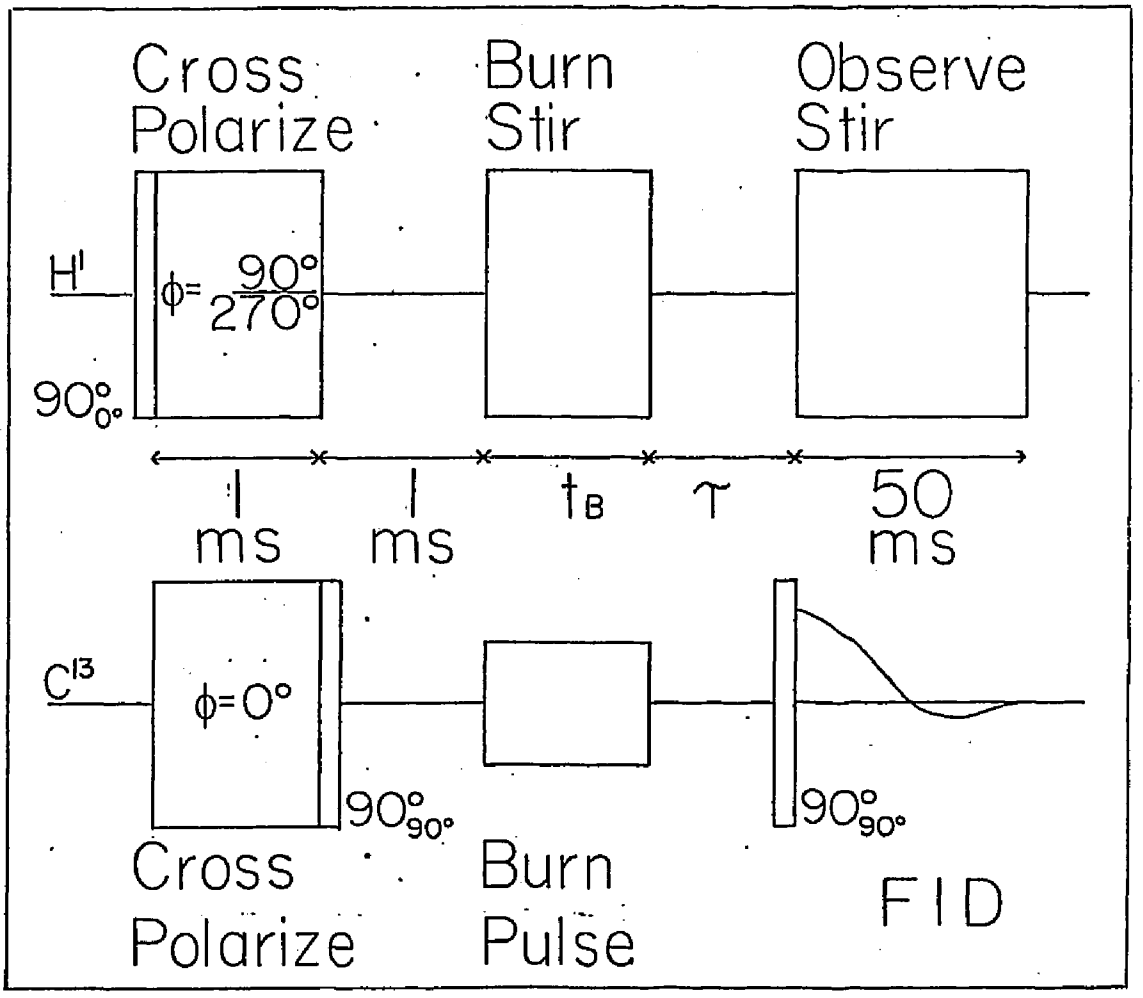

Figure 4: Pulse sequence used in hole-burning experiments for protons (upper) and C^{13} (lower). The time τ is typically between 10^{-2} and 2×10^{2} s.

shorter than T_1 carbon, and the cross-polarization results in an enhanced M_z for the carbons.

The phase of the proton spin-locking pulse was shifted by 180 degrees every other repetition of the experiment. This means the proton spin temperature alternated between $\pm$ .2K (Red55, Sli61). Consequently the carbon magnetization following the 90 degree store pulse was aligned parallel and then antiparallel to H_0. The data collection scheme took the resulting signal inversion into account by multiplying alternate signals by minus one in software. For large values of the waiting interval, τ, the initially negative spin temperature traces will have recovered to positive temperatures (Boltzmann equilibrium). Hence for two pulse sequences with $\tau \gg T_{1C}$, the averaged spectrum is zero. And as a result, the T_{1C} effects cause the intensity of the carbon-13 to approach zero for large waiting intervals.

The 1 ms wait following the cross-polarize sequence is to allow any perpendicular (to H_0) components of the carbon magnetization to dephase. Because the protons are unstirred, $H_{IS}^D \neq 0$ and so the dephasing of the carbons is complete in ~ 100 μs.

4.3.2 Hole-Burning

The next part of the hole-burning pulse train is the burn pulse (Blo48) It is a long weak pulse of small amplitude that irradiates the carbons. The pulse amplitude and length are adjusted so that $\gamma H_1^b t_b = \pi$ or $\pi/2$, where H_1^b is the amplitude of the burn pulse and t_b is the length. During the carbon burn pulse the protons are vigorously spin-stirred to remove the IS dipolar interaction. The spin-stirring leaves

the carbon spectrum composed of isochromats which are distingushed only by their chemical shifts.

The idea behind selective saturation, burning a hole, is that a long weak pulse has a narrow fourier power spectrum. So by using long pulses, only the magnetization in a narrow frequency window is significantly nutated. The angle of nutation of the magnetization at the rf driving frequency is $\theta = \gamma H_1^b t_p$.

To calculate the effect of the pulse, one uses the Bloch equations in the rotating frame. Initially, the components of the carbon magnetization are $M_x = M_y = 0$, and $M_z = M_0$. Using the approximation $T_1 = T_2 = \infty$, we have

$$\frac{d}{dt} M_i = \gamma(\bar{M} \times \bar{H})_i$$

for i = x, y, or z, denoting the components in the rotating frame where the rotating frame magnetic field $\bar{H} = H_1 \bar{i} + h \bar{k}$. Solving for $M_z(h,t_p)$

$$M_z(h,t_p) = M_z(h,0) + \frac{H_1 M_z(h,0)}{\left[H_1^2 + h^2\right]^{1/2}}\left[\cos(\gamma\{h^2 + H_1^{b2}\}^{1/2} t_p) - 1\right] \tag{58}$$

the equation that describes the hole shape in terms of h, the off-resonance field. It is apparent that the larger the rf field (H_1^b) is the broader the hole will be. For a given H_1^b, the shorter t_p (for $t < \pi/\gamma H_1$), the shallower the hole will be. Hence we can tailor the hole, controlling both its width and depth. The carbon burn pulse used in these experiments was typically 1.5 to 15 ms long and its amplitude

was between 0.25% and 0.025% of the normal (unattenuated) rf amplitude. Consequently, the holes varied from 70 Hz to 450 Hz FWHM. The lower limit was presumably determined by the C^{13}-C^{13} dipolar interaction.

The delay following the burn pulse allows for the redistribution of the magnetization due to molecular reorientations (spectral diffusion). Following the delay a carbon 90 degree pulse is used to inspect the magnetization. The protons are spin-stirred during the recording of the carbon signal to remove once more the IS dipolar interactions.

4.4 SPECTRUM

As previously mentioned, the carbon spectrum (during proton spin-stirring) is composed of isochromats whose frequency is determined by anisotropic chemical shift. This means that there is a connection between the resonance frequency of the carbon spins and the molecular orientation relative to H_0.

The unburned spectrum for glycerol is found to be approximately a uniaxial powder pattern. Unburned spectra for two temperatures are shown in Fig. 5. They were taken using the same pulse sequence as discussed earlier, but with no burn pulse.

The spectra taken between 122 K and 203 K, for all practical purposes, are identical. We conclude that the molecular motions in this temperature range are either much faster or much slower than the rigid linewidth due to the anisotropic chemical shift $\Delta\omega_{RL}^{CS}$ (1 KHz). Examples of faster motions are vibrations and librations. Slower motions are translations and reorientations.

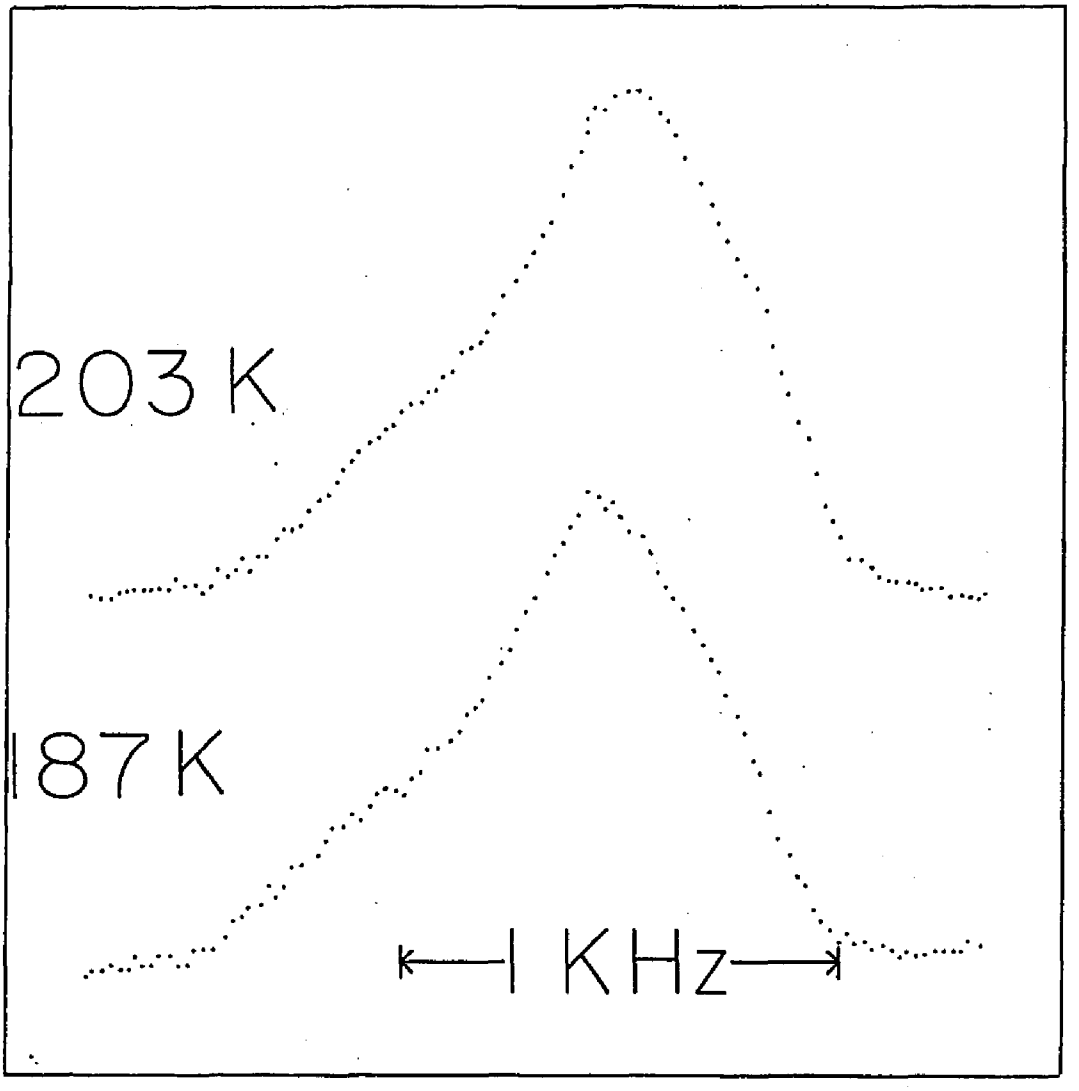

Figure 5: C^{13} powder-pattern spectra of glycerol obtained with proton spin decoupling. The high frequency, low field end of the spectra is to the right.

The glycerol spectra are due to two carbons in different chemical positions, end carbons and middle carbons. Liquid spectra show two lines with approximately a 2-to-1 ratio of areas, as expected. The separation of the centroids of these liquid lines is only 10 ppm or 200 Hz (f_0 for C^{13} is 20.846 MHz). Consequently the resonances from these two carbons overlap severely in the solid. The approximate shape of the combined resonances is a uniaxially symmetric powder pattern.

The overall chemical shift anisotropy of glassy glycerol is 50 ppm or 1 KHz, which agrees well with the reported anisotropies of OH carbons in methyl and ethyl alcohol (Pin72a). The distinct edges in the theoretical powder pattern, Fig. 1, are not seen in the glycerol spectra. This indicates that there is an additional source of broadening (Blo53), of ~ 250 Hz. The additional broadening is inhomogeneous. We burned very narrow holes (70 Hz FWHM) and measured T_2, using the Carr-Purcell pulse sequence ($90_{90} - \tau - 180_0 - 2\tau - 180_0 \ldots$) (Car54, Mei58). The result was T_2 = 15 ms, or a homogeneous linewidth of 21 Hz FWHM. Inadequate proton spin-stirring cannot be the source of the additional broadening because the IS interaction would produce homogenous broadening. However, in a liquid glass there is a distribution of molecular environments due to the disorder. In amorphous polymers this yields inhomogeneous C^{13} linewidths of ~ 40 Hz at ~ 20 KG, our DC field (Sch77). This is too small to be the source of our broadening.

Glycerol, like any organic molecule will have internal degrees of freedom. Examples are, rotations about C-C and C-O bonds. Since the chemical shift will depend not only on the orientation of the C-C-C

backbone, but also on these internal coordinates, we conclude that there are distributions of internal coordinates that are causing additional broadening.

The overall spectrum is approximately a uniaxial powder pattern. Consequently, the connection between frequency and orientation is still applicable. For uniaxial powder patterns the relationship between ω, the resonance frequency, and θ, the molecular orientation, is given by equation 48,

$$\omega(\theta) - \omega_0 = \omega_0 \Delta\sigma(\cos^2 \theta - 1/3),$$

where ω_0 is the isotropic (liquid) resonance frequency, $\Delta\sigma$ is the strength of the shift anisotropy, and θ is the angle between some molecular axis and H_0. So by saturating the spectra between ω' and ω'' we tag the molecules between θ' and θ'', where $\omega'' = \omega(\theta'')$ and $\omega' = \omega(\theta')$.

4.5 HOLE RECOVERY

During the interval τ between the carbon burn and inspect pulses, molecules will reorient. This reduces the intensity of the spectrum at the frequency, corresponding to the molecules new orientation. By detailed balance, a tagged molecule reorienting out of the hole, is balanced by a molecule (most likely unburned) reorienting into the hole. This activity results in increasing intensity in the initially burned region. The net effect of molecular reorientation will be to spread the hole into the unburned part of the spectrum while maintaining the total integrated intensity of the line. This is spectral diffusion.

By burning a very narrow hole the orientation of some molecules is specified as θ_0 at t_0. By observing the recovery of this narrow hole, the single-particle, two-time orientational correlation function can be determined. That is, by observing the spectrum at $t_0 + \tau$ one finds a picture of the correlation function $P(\theta_0, \theta; \tau)$. For a reorientation or a series of reorientations to visibly change the NMR spectra the reorientations must carry a spin from inside to outside the hole. This requires that the molecule reorient so that the average spin changes frequency by a minimum of half the hole width. By comparing the recovery of initially varying hole widths, one can deduce the size of the mean angular reorientation. For molecules reorienting by small stochastic jumps (random walk on a sphere), the effect on the spectrum will be to 'erode' the edges of the hole, broadening it while it becomes shallower, Fig. 6. This is because small reorientations will only connect frequencies near each other. Consequently in the limit of small angle motion, initially broad holes will recover slower than initially narrow holes.

The other limit is large, angular jumps. That is, a molecule is equally likely to have any orientation after a jump. The effect of this motion on the NMR spectrum will be to spread the hole uniformly across the spectrum. Hence, the depth of the hole will decrease at the expense of the rest of the line, and the hole will recover without changing shape, Fig. 6. The signature of large angle motion is that the FWHM of the hole will be independent of τ, the waiting interval, and holes of different initial widths will recover at the same rate.

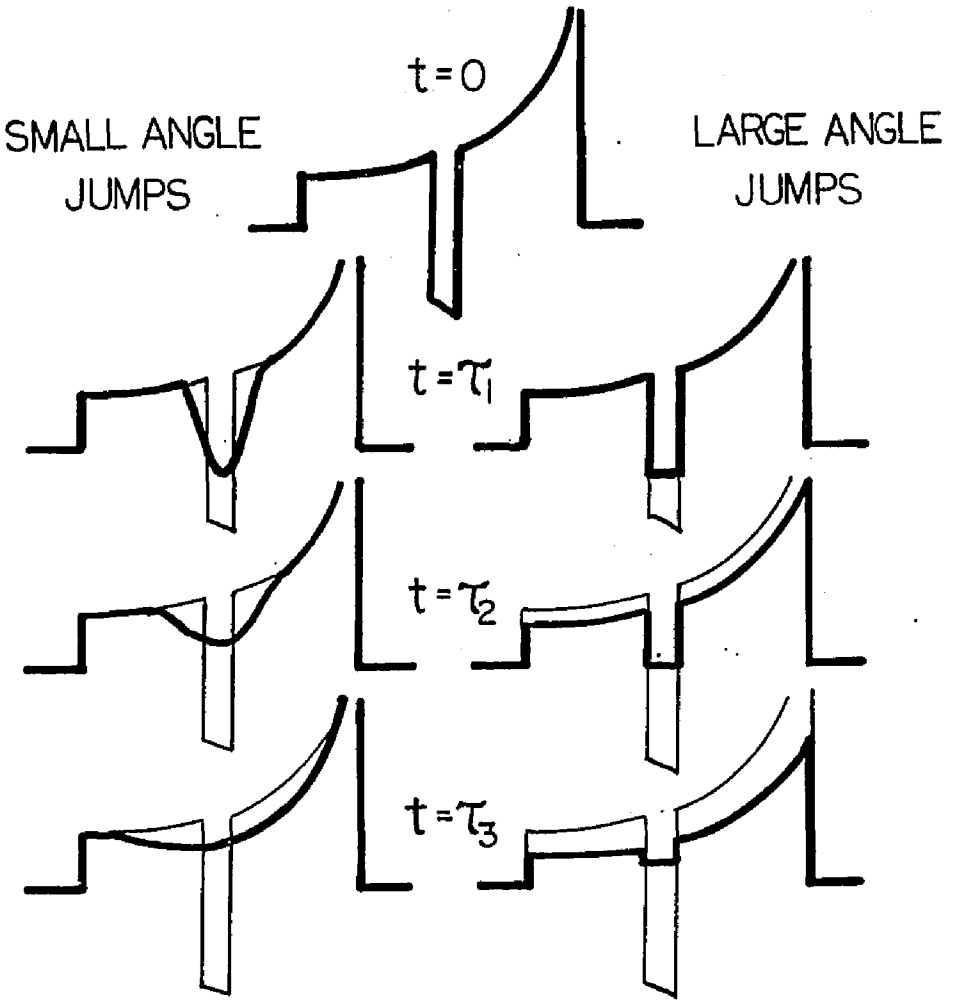

Figure 6: Expected spectral diffusion for large- and small-angle molecular reorientations. The waiting interval is increasing for descending pictures.

A proviso must be attached to the last statement. The broader the hole, the more likely it is that a reorientation will carry the spin right back into the hole. This 'target area' effect will be seen mainly in the large holes, which should recover slightly slower than narrower holes.

Because of dilution (C^{13} is 1.1% naturally abundant) the carbon spins are very weakly coupled. So hole recovery follows the change in resonance frequency of individual, uncoupled spins. Therefore the entire relaxation function is observable, not just the mean relaxation time, as is the case in strongly coupled spin systems (systems of large γ and 100% abundance). This is particularly useful in the study of disordered materials where distributions of relaxation times are frequently encountered (McC67). After a hole is burned the entire line relaxes towards its Boltzmann equilibrium line shape with a time constant T_1. The effects of T_1 put a limit of the longest observable reorientation time because after a few T_1 the hole becomes unobservable. However T_1 processes are easy to separate from spectral diffusion in the data. Spin-lattice relaxation will change the total integrated intensity of the line, whereas hole recovery will leave the total intensity unchanged. Therefore the effect of T_1 relaxation can be eliminated by simple scaling, up to the limit of signal to noise. The short time limit of hole-burning is when the molecular reorientation rate ω_r becomes greater than $\Delta\omega_{RL}^{CS}$, the rigid lattice powder pattern linewidth. When ω_r exceeds $\Delta\omega_{RL}^{CS}$, motional narrowing sets in, destroying the dependence of ω on θ, equation 48 (Spi74a, Spi74b, Meh76). That is, the picture of well-defined isochromats relating to well-defined angles becomes inaccurate.

Consequently the window in which ω_r is observable by spectral hole-burning is $\omega_{RL}^{CS} > \omega_r > T_1^{-1}$. For glycerol the limits of spectral hole-burning are 10^2 Hz $> \omega_r/2\pi > 10^{-2}$ Hz, a rather large window. Hence this technique measures slow motions, slower than accesible by most other relaxation techniques. It can also be used to determine the angular step size and the distribution of motional rates.

As mentioned before, the width and depth of a hole could be tailored to our specifications, as predicted by the Bloch equations. In Fig. 7 are pictured the three types of holes used. The qualitative features of the holes (when observed for short τ) agree with the calculated features, equation 58. Indeed the small dimples in the center spectra (medium hole) at about $\pm$ 300 Hz from the hole's center, are due to the damped cosine term in the Bloch equations. We also note that the gross features of the Bloch equations are obeyed. Short 'intense' pulses produce broad holes and long, weak pulses give narrow holes. The center of the broadest hole was intentionally made to reach only to the baseline, to give a positive total area to the spectrum. The narrowest holes (t_p = 12 ms) could only force the magnetization to the baseline. Slightly longer pulses did not deepen the hole, but only partially saturated a wider section of the line. This is because T_2, the C^{13} linewidth, is 15 ms.

The holes, for future convenience, will be named narrow, medium and broad. A medium hole at 198 K (43 K above T_g) is shown at various stages of recovery, Fig. 8. The vertical lines are the FWHM determined from three shortest time holes (τ = 0.025, 0.1, and 0.4 s). It is apparent that the hole is recovering without changing shape. In fact this

is true of all three hole sizes. The decrease in total intensity is due to carbon spin-lattice relaxation, that occurs during the waiting time τ.

We conclude from the τ independence of the hole width that the molecule reorientations in glycerol are large angle jumps. In fact, the time independence of the broad hole width, which is ~ 45 degrees FWHM, puts a lower limit of 45 degrees on the average reorientation angle of the glycerol molecules. (The entire spectrum is 90 degrees wide. So the broad hole, being half the linewidth, is ~ 45 degrees FWHM.)

The measurement of the hole depth, in the presence of spin-lattice relaxation, requires some subtlety. Since diffusion of the hole into the line does not change the total intensity of the line, any changes in the total intensity are due to T_1 processes. If the T_1 processes are orientationally independent, that is, if the line decays uniformly, T_1 effects can be removed by simple scaling of the total spectra. In a series of uninteresting experiments T_1 was shown to be independent of frequency. The scaling factors can be determined by measuring T_1 for carbon and multiplying each spectra by exp (τ/T_1). The scheme we used for determining the scaling factors was to measure the decay of the total intensity of burned spectra for each τ used in the hole recovery experiment. The two procedures are identical, but the second method was easier to automate even if it used more time. In general, τ was kept short enough that the scaling factors were less than 2.0 for signal to noise considerations.

A general method of measuring the hole recovery is to subtract scaled, burned spectra from an appropriately sized unburned spectra.

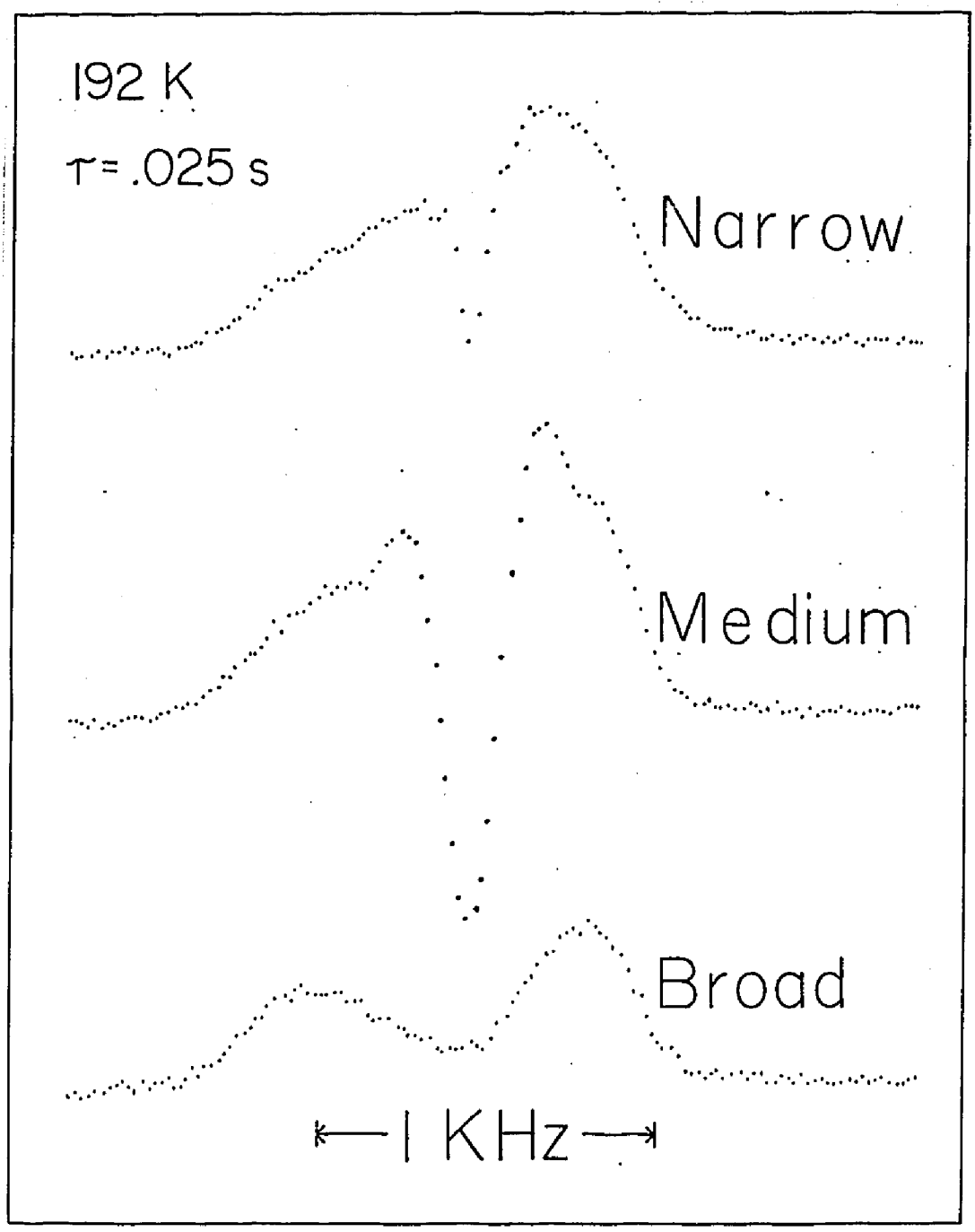

Figure 7: Holes of three widths burned into the spectrum of Fig. 5. The value of τ (see Fig. 4) is 0.025 s.

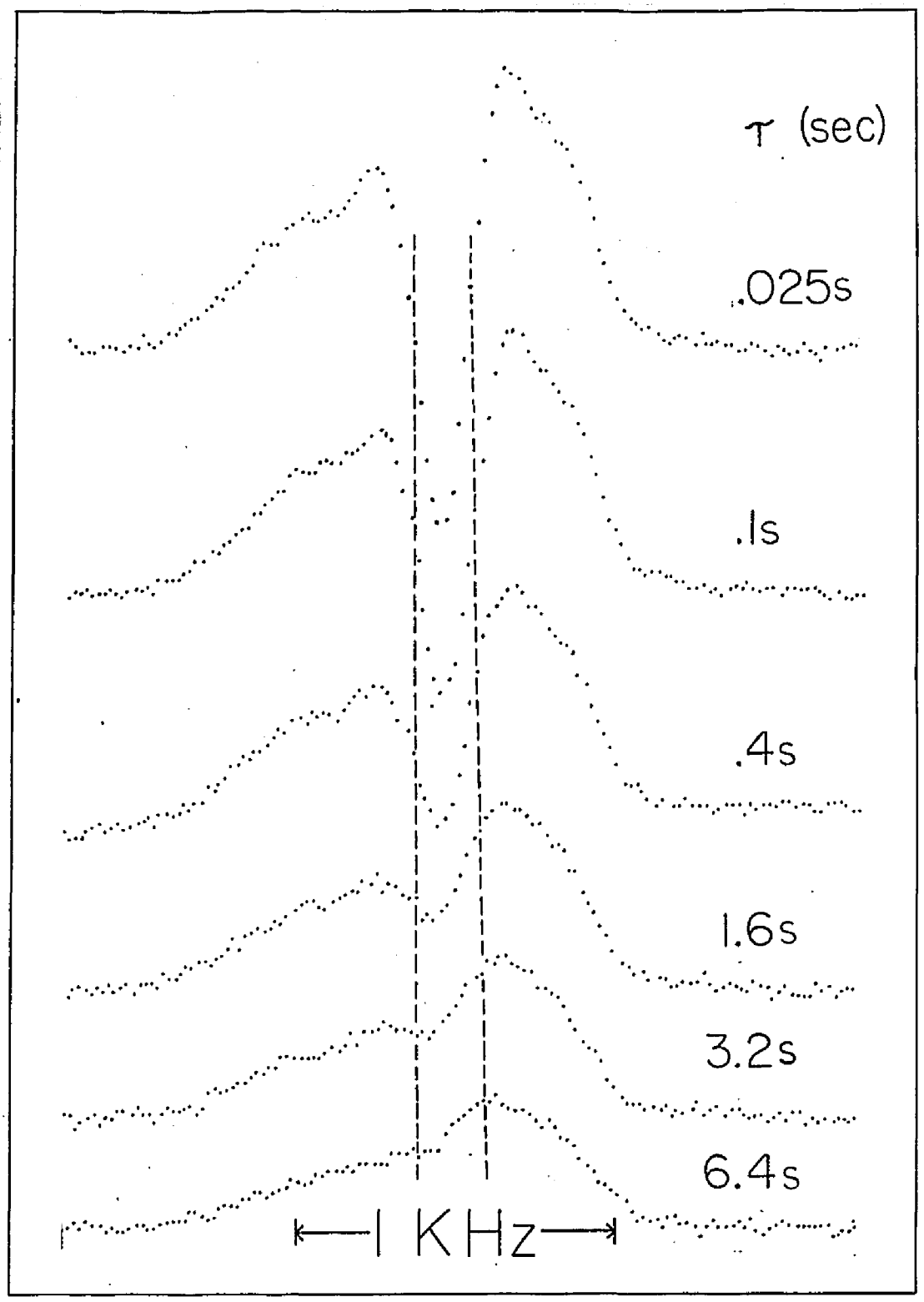

Figure 8: Recovery of a medium-width hole in C^{13} glycerol line at 198 K. The hole width remains constant through the recovery, indicating large-angle motions. The vertical lines are FWHM of the hole.

Doing this for various values of τ will give a picture of just the hole as it recovers. However, in glycerol the holes recovered without changing shape, so the following (fairly straightforward) mathematical technique was used. The burned spectra were multiplied by a rectangular filter function that was one in the middle of the hole, minus one on the shoulders of the hole, and zero elsewhere. We required that this function, when applied to the unburned spectra, gave a net area of approximately zero. The product of the filter function and the scaled burned spectra were integrated. The resulting value was the hole depth. The rectangular function was determined for each temperature and then held constant for each of the spectra taken at various values of τ.

4.6 RESULTS

Using this technique for determining the hole depth, we measured the decay of the holes. The decay curves at two temperatures for different-sized holes are shown in Fig. 7. Note that the time scale is logarithmic.

Consider the 192 K decay curve. The narrow hole recovers fastest. It reaches 50% of its initial depth in 10 s. The medium hole is slightly slower. It reaches 50% of its initial depth in 13 s or recovers to 55% in 10 s. The broadest hole is the slowest, reaching 50% in 26 s or 62% in 10 s. Hence motions that relax a narrow hole will relax a broad one, and vice versa, except for target area considerations. Therefore we conclude (again) that the reorientations are large angle jumps of at least 45 degrees, the angular width of the broadest hole. This result agrees with other NMR work on deuterated glycerol by Wolfe

and Jonas (Wo179), and the interpretation of Rayleigh scattering, dielectric, and volume relaxation data (Pin68) that all favored large angle motion.

The data in Fig. 9 are non-exponential as can be seen from the dashed line, which is a simple exponential,

$$\tau = A \exp -\{t/\tau_c\}. \tag{59}$$

The constants A and τ_c were determined so that the exponential would pass through the medium hole data at 0.1 s and 12.8 s. The exponential misses the medium hole data badly. But the solid line, a Williams-Watts (W-W) function (Wil70, Wil71),

$$\tau = \exp -\{t/\tau_c\}^{\beta}, \tag{60}$$

is an excellent fit to the data. Non-exponential recoveries are common in glasses. Presumably, molecules in a glass have a distribution of environments and barrier energies, (there are other interperations of this) (McD63, Lit63). The parameter β in the W-W function was determined to be 0.5 ± 0.1 by fitting all the data. The non-exponentiality of the W-W function is determined by β, where β is a measure of the width of the distribution of relaxation times. Setting $\beta = 1$ gives a single relaxation time and letting β approach zero makes the distribution become infinitely wide. Our value of $\beta = 0.5 \pm 0.1$ is not very precise. But a more accurate determination would require hole recovery data over at least another order of magnitude in time. Hole recoveries, extending over such large time intervals, are not possible because of the limits placed on τ by T_{1c}, $\Delta\omega_{CS}^{RL}$, and signal-to-noise.

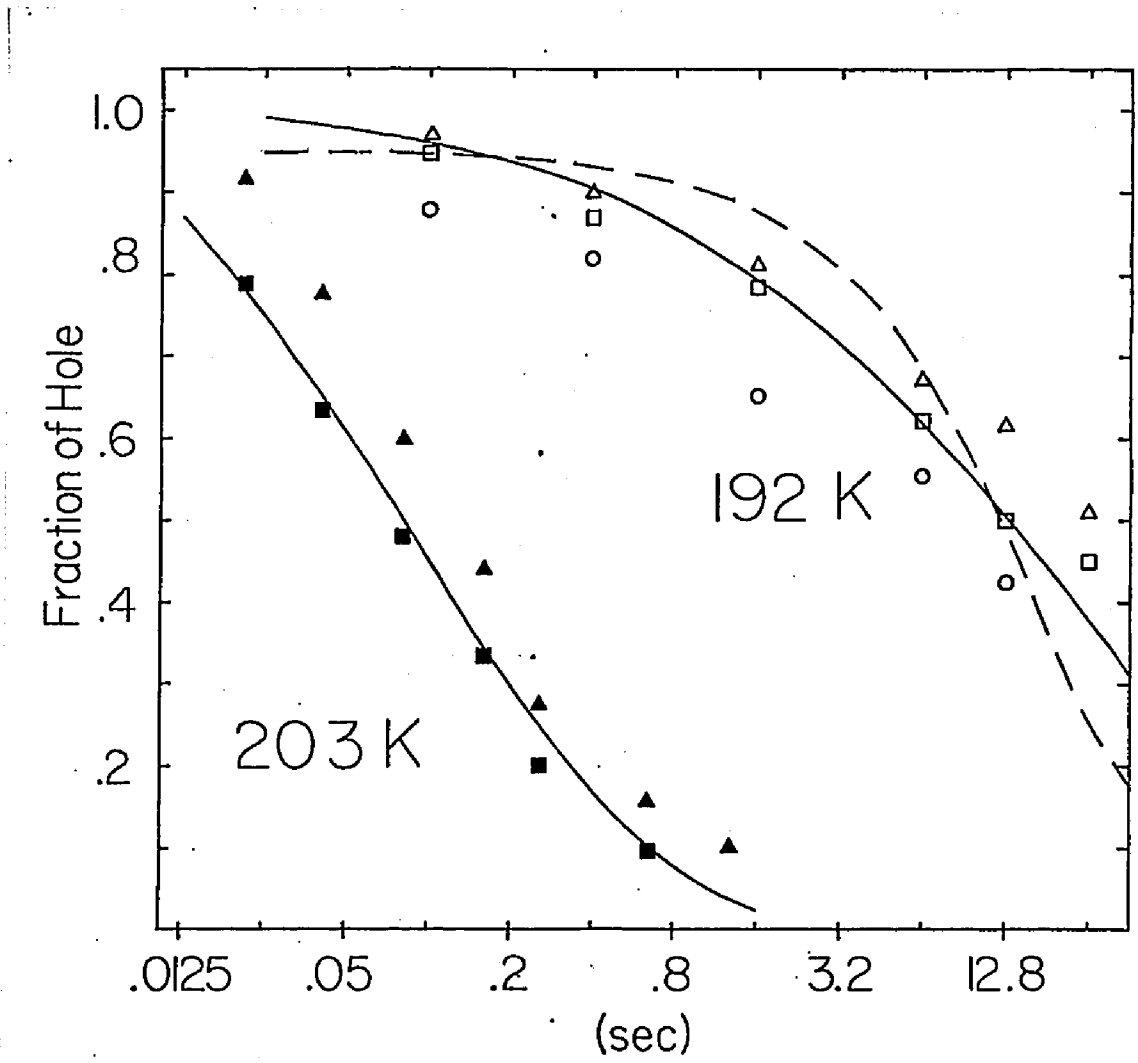

Figure 9: Hole recovery data at 192 K (open symbols) and 203 K (filled symbols). Narrow (o), medium (□,■), and broad (△,▲) holes were used. The solid curves are fits to the medium hole data.

An excellent discussion of the W-W function, its implications, and the fitting of experimental data with it was done by Lindsay and Patterson (Lin80). They compared the Cole-Davidson (C-D) function (another analytical distribution function) to the W-W function. The C-D function is (Dav51a, Dav51b)

$$g(\tau) = \sin a\pi/\pi(\tau/\tau_o - \tau)^a$$
$$\text{for } \tau < \tau_o$$
$$= 0$$
$$\text{for } \tau > \tau_o, \qquad (61)$$

where the parameter 'a' determines the width of the distribution of correlation times. A numerical comparison of the functions yielded the following relationship between β from the W-W function and 'a' from the C-D function,

$$\beta = 0.976a + 0.144$$
$$\text{for } 0.2 < a < 0.6$$
$$\beta = 0.683a + 0.316$$
$$\text{for } 0.6 < a < 1.0. \qquad (62)$$

Previous dielectric experiments on glycerol fit their data using the C-D function with 'a' = 0.6 (Dav51b, McD62). Using the above equations, this corresponds to $\beta = 0.6 - 0.7$, in tolerable agreement with our result $\beta = 0.5 \pm 0.1$. For hole recovery data, the average reorientation rate ω_R may be (arbitrarily) defined as the inverse of the value of τ at which the medium hole has recovered to 50% of its ini-

tial depth. Because the three different hole sizes recover at essentially the same rate, this is a sensible definition. Using this definition to determine the reorientation rate, the values of $\log_{10} \omega_R$ are plotted in Fig. 10 as a function of inverse temperature. Also plotted are the values of ω_R as determined from dielectric relaxation (Dav51b, McD62) and NMR quadrupolar relaxation (Wol79) experiments. The dielectric workers, as mentioned earlier, used the C-D distribution function. They reported τ_0, the limiting value of the C-D distribution, as the characteristic reorientation time. Lindsay and Patterson showed that the average reorientation time $\bar{\tau}$ for a C-D distribution is given by $\bar{\tau} = a\tau_0$. It is $\omega_R = 1/\bar{\tau}$ that we plotted in Fig. 10 for the dielectric data.

Our data extends the previous determination of ω_R to much lower frequencies. The hole recovery data fits smoothly onto the other data. This indicates that we measured the same motion as the other techniques did.

The relaxation curve, Fig. 11, becomes steeper as the temperature is reduced. This behavior is common in materials that undergo glass transitions. Such data is usually fit with the Williams-Landau-Ferry (WLF) (Wil55) or Vogel-Tammann-Folcher (VTF) equation given by

$$\omega_R(T) = \omega_0 \exp -\{(E/k)/(T - T_0)\}. \tag{63}$$

The constants used in the fit, Fig. 10, are $\omega_0 = 7.52 \times 10^{15}$ s^{-1} $(E/k) = 2694K$, and $T_0 = 123.7K$ (McD62). The fit of the data extrapolates through 10^3 s at 186 K, scale 10^3 s) of the glass temperature, T_g

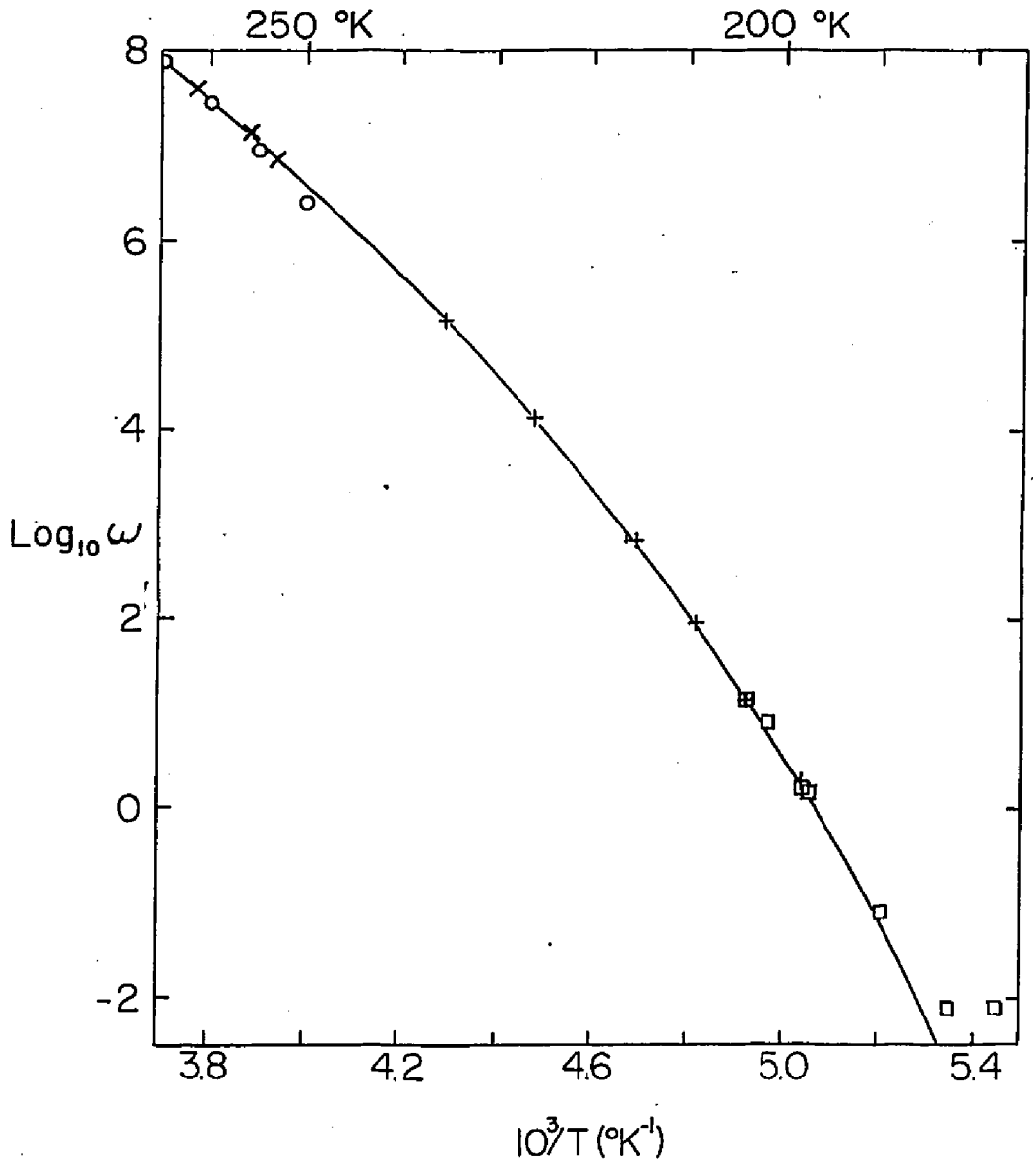

Figure 10: Reorientation rate ω_R as a function of temperature. The hole recovery data reported here (□) appear with the dielectric data (+ (Dav51b), x (McD62)) and NMR data from deuterium T_1 (o (Wol79)).

= 185 K (Gib2 Par27). This shows that the motions measured by hole-burning are also responsible for the glass transition. The fitting parameters are due to the dielectric workers. We converted their fitting parameters for τ_0 to ω_R for plotting in Fig. 10.

As mentioned previously, the broadening in the powder pattern occurs because the NMR spectrum is sensitive to internal coordinates as well as to the orientation of the carbon backbone. The question arises whether the hole-burning data is merely following changes of these internal coordinates. But this possibility is eliminated by the observation that the broad holes recover nearly as fast as the narrow holes. The broad holes, being 450 Hz wide, are wider than the additional broadening (~ 250 Hz). So they would recover slower than the narrow holes, if internal rearrangement was the dominant mechanism of hole recovery. The internal rearrangements almost certainly involve OH group reorientations. Wolfe and Jonas (Wol79), from their deuterium NMR data, concluded that OH group motion occurs at essentially the same rate as the overall molecular rotations. Because of this and the excellent agreement of our data and the data from other techniques, we conclude that with hole-burning we are indeed following overall molecular rotations.

In Fig. 10 the average hole recovery time becomes independent of temperature at 189 K. At low temperatures the reorientation rate becomes so slow that a competing temperature independent mechanism becomes dominant. This is undoubtedly due to spin-spin interactions between the carbon-13 spins. As mentioned earlier, the existence of the chemical shift anisotropy (~ 1 KHz) lifts the degeneracy between the states

$|m_1,m_2\rangle = |+\ -\rangle$ and $|-\ +\rangle$. This will inhibit the C^{13}-C^{13} flip-flops, which the C^{13}-C^{13} interactions would cause (Van79). In addition, during the waiting interval τ, the protons are not spin-stirred, causing the spin evolution during this interval to be complicated.

4.6.1 Spin-spin Relaxation Time

We also measured the spin-spin relaxation time T_2 for the C^{13} spins using the Carr-Purcell sequence ($90_{90} - \tau - 180_0 - 2\tau - 180_0 \ldots$) (Car54, Mei58) for the carbons, while spin-stirring the protons. Five different repetition rates for the refocusing pulses were used, ranging from 130 pulses/s (τ = 7.7 ms) to 1500 pulses/s (τ = 660 μs). The data from two pulse densities are shown in Fig. 11.

The difference in the results for the two pulse densities is unexpected. It is not known whether this is due to H_1 inhomogeneity or the attainment of a Hartmann-Hahn match during the refocusing pulses, (and the resulting 'leakage' of the decaying C^{13} magnetization) (Ear79). Even so, the T_2 values are not strongly dependent on the pulse densities and are found to be temperature independent below 200 K. For higher temperatures, the stochastic motion partially defeats the coherent spin-stirring and the carbon refocusing pulses. Consequently above 200 K, T_2 decreases with increasing temperature. The temperature independent value of T_2 = 15 ms indicates the C^{13}-C^{13} dipolar linewidth (the isochromat width) is ~ 21 Hz, as previously mentioned. The knee in T_2 at ~ 200 K indicates that ω_R is becoming equal to or greater than the inverse of the rigid lattice T_2, about 70 s^{-1}.

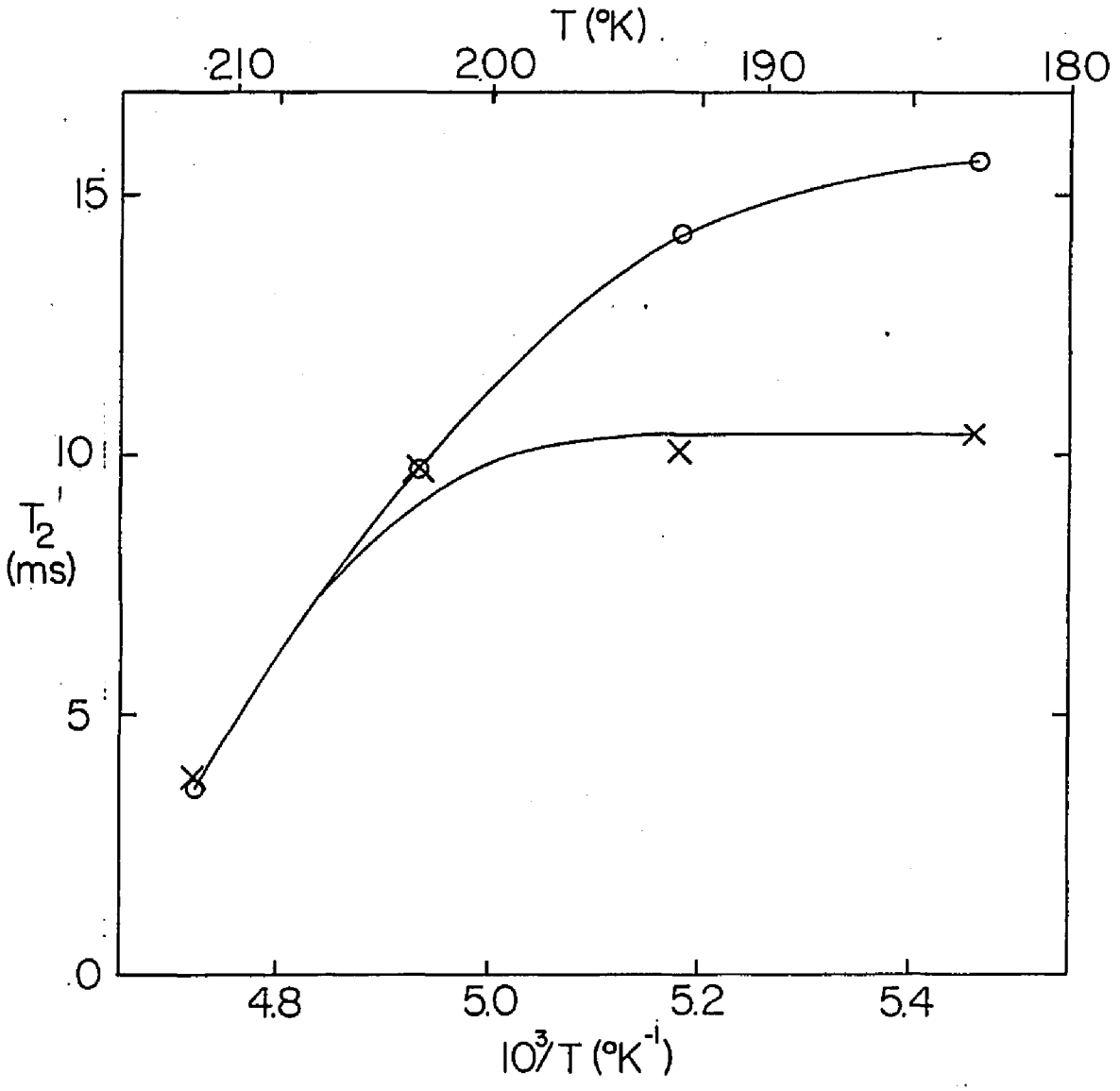

Figure 11: T_2 values measured with Carr-Purcell sequences of 800 pulses/s (x) and 267 pulses/s (o). The solid curves are guides to the eye.

4.7 OTHER TECHNIQUES

Waugh et al. have developed methods of measuring motions in solids in which the defeat of the coherent spin-stirring by the stochastic motions produces line broadening of the dilute spin species (Saw80, Rot81). These experiments are done in the presence of spin-stirring of the abundant spins, with and without magic angle spinning. These techniques use the magnetization while it is perpendicular to H_0 and, consequently, only motions faster than T_2^{-1} (the isochromat width under spin-stirring) are detectable.

Another closely related technique is the three pulse sequence used by Lausch and Spiess (Lau80, Spi80) to measure spectral diffusion in deuterium NMR. The NMR spectrum of deuterium is also orientationally dependent (the orientation of the electric field gradient, rather than the chemical shift tensor). The three-pulse sequence produces a sinusoidal modulation of the spectrum (many holes) of various periods. This modulated spectrum is stored along H_0, so the detectable motions must only be faster than T_1

4.8 GLYCEROL CONCLUSIONS

The spectral hole-burning experiment used here to study the molecular motions in glycerol followed the molecular reorientation rate ω_R from $10^{-2}$to 10^2 s^{-1} for temperatures just above T_g. Analysis of the hole recovery data directly showed that the mean reorientation angle in supercooled glycerol is greater than 45 degrees, in agreement with other glycerol studies. Spectral hole-burning allows the entire relaxa-

tion function to be observed, unlike many other relaxation techniques. We found that there exists distribution of reorientation times in glycerol. The distribution could be fit with the Williams-Watts distribution function, using $\beta = 0.5 \pm 0.1$, for all the temperatures we studied. This is in fair agreement with the width of the distribution as deduced from dielectric experiments.

In many orgnic solids the density of protons and carbons are about the same as in glycerol. So if the carbon linewidth is dominated by anisotropic chemical shift, spectral hole-burning should be an excellent technique for the study of slow molecular reorientations.

Chapter V

THE CYCLOHEXANOL EXPERIMENT

5.1 BACKGROUND

Cyclohexanol, $C_6H_{11}OH$, freezes from the melt into a rotor crystal, a solid that possesses translational order and orientational disorder accompanied by rapid molecular reorientations (Tim61). Like many molecules that form rotor crystals (e.g. cyclohexane and adamantane), cyclohexanol is globular in shape (especially in its chair configuration) and has a low entropy of fusion, 0.7 R (Ada68). The lattice structure of the rotor phase is face-centered cubic, with a lattice parameter of 0.88 nm and four molecules per unit cell (Gre69a, Cec80, Dun61).

There are two stable solid phases of cyclohexanol, crystal I, the rotor solid, and crystal II, an orientationally ordered phase in which the molecules are not free to rotate. Solid cyclohexanol also has several metastable phases, a relatively stable modification III and precursor phases II' and III'. The sample transforms from I to II or III via II' or III', depending on the sample's thermal history (Ada68).

Crystal I is stable between 299.1 K and 265.3 K and is readily supercooled through the I-II transition. The effect of supercooling is to slow the molecular reorientations until, at 150 K (T_g), a glass transition is observed in specific heat measurements. The size of the step-like decrease in the specific heat (ΔC_p = 32 J/mole/K) at the

glass transition (Ada68, Kel29), is somewhat smaller than typical step sizes in glassy organic liquids (in glycerol ΔC_p = 79 J/mole/K) (Gib23). In common with other glasses, the entropy of phase I does not go to zero at zero temperature. Instead it retains a residual value of 4.72 joules/mole-K (Ada68). By comparison, the ordered phases II and III have zero entropy at 0 K. X-ray measurements indicate no change in the long-range crystal structure between the high temperature rotor phase at 290 K and the glassy crystal at 120 K (Cec80, Ots55). Hence, the names rotor crystal, supercooled rotor crystal, and glassy crystal all refer to the same phase (I).

The presence of the OH group makes some kind of glass formation likely in cyclohexanol. Many alcohols form hydrogen bonding networks resulting in viscous liquids and a tendency toward glass formation (Par27). Indeed, liquid cyclohexanol at the melt is viscous. The globular shape of the cyclohexanol molecule leads to rotor crystal formation (Tim61). The combination of rotor crystal formation and glass formation tendencies produce a substance that forms an orientational glass in the supercooled rotor phase.

We note that glassy liquid cyclohexanol (supercooled liquid) has also been produced (Cec80), but does not form as readily as the glassy crystal (supercooled rotor crystal).

The relationship between the viscosity and the tendency towards glass formation has long been known. The rotor phase of cyclohexanol may be thought of as rotationally quite viscous. The rotational correlation rate in the solid at the melt is ~ 5 x 108 s^{-1}, as deduced from our T_1 measurements. This is quite low compared to other rotor crys-

tals at their melts (Bod79), such as 5 x 10^{10} s^{-1} in cyclohexane (ORe72) and 6.3 x 10^{11} s^{-1} in adamantane (Res69). The comparatively slow rotations in cyclohexanol in the warm rotor solid indicate that glassy crystal formation is likely.

5.2 EXPERIMENTAL

The cyclohexanol used in these experiments was Fisher reagent grade. Several different samples in various diameter glass tubes (13 mm, 6 mm, 4 mm, I.D.) were used. The small diameter tubes were used in the $T_{1\rho}$ experiments, which required high H_1. All the samples were exposed to CaO or $MgSO_4$ and Linde sieve number 4 for several days to remove any water (cyclohexanol readily absorbs atmospheric water). The samples were then sealed into tubes with 0.5 atmosphere of dry N_2 gas. This gas aided thermal contact to the sample and prevented arcing from the rf electric fields. These problems become important in cold, low vapor pressure samples. The removal of traces of water was recommended to us by Prof. H. Suga to increase the metastability of the supercooled cyclohexanol I (Sug81). Two of the samples were purified by fractional distillation, but all of the samples gave identical results. One of the samples had a small amount of CaO sealed into the tube as a permanent water getter. This sample tended to transform into other unwanted phases more readily. Perhaps the CaO provided nucleation sites to start the phase change.

The 13 mm and 6 mm tubes contained a thermocouple well, a second smaller tube with the bottom sealed, dipping into the center of the sample. A copper-constantan thermocouple at the bottom of the well

measured the sample temperature. The thermocouple was used to confirm that the sample had not transformed into other phases (Ots55). The exothermic transformation to the more stable phases was readily seen on a chart recorder connected to the thermocouple microvoltmeter. The low temperature ($T < 100$ K) T_1 measurements used a (Lakeshore) carbon-in-glass resistance thermometer immersed in the flowing He gas to measure the temperature of the sample.

Whenever evidence (abnormally long T_1 or the thermocouple readout) suggested that the sample was transforming, the temperature was raised to between 285 K and 295 K. The sample was allowed to completely anneal and transform back to phase I before it was rapidly cooled to the desired temperature. The cooling rate was typically 20 K per minute.

5.3 RESULTS AND DISCUSSION

The spin-spin relaxation time T_2 and the second moment M_2 are plotted in Figs. 12 and 13 along with M_2 determined from continuous wave methods by Eguchi et al. (Egu75). The relaxation time T_2 was determined by measuring the time for the signal to decay to e^{-1} of its maximum amplitude. For low temperatures ($T < 175$ K) a solid echo ($90_0-\tau-90_{90}$) was used to avoid the receiver blocking of the zero time signal. FIDs were used in the region of extensive motional narrowing ($175\text{ K} < T < 210\text{ K}$) because the solid echo amplitude became very small. FIDs were also used in the region of the rotationally fully narrowed line ($T > 210$ K), because the receiver blocking is short compared to T_2. The second moment (Abr78) was determined from the second derivative at the peaks of magic echoes and solid echoes (Low57). Both

gave results that agree with the continuous wave results. As expected, magic echoes could not be formed in the region of extensive motional narrowing (175 K < T < 210 K) because of the stochastic modulation of the dipolar interactions.

We found that the simple pulse sequence for magic echo formation of Bowman and Rhim ($2\tau_0$-90_{90}) (Bow82) can be improved by using the sequence (τ_0-τ_{180}-90_{90}) as suggested by R. E. Norberg (Nor82). The times τ are typically 25 to 50 μs and the magic echo forms at time τ after the 90 degree pulse. The insertion of the 180 degree phase shift eliminates the reduction in the echo amplitude due to the dephasing of the magnetization about an inhomogeneous H_1. It also eliminates the dependence of the echo's phase on the pulse length τ. Magic echoes were first observed and explained by Waugh and co-workers (Rhi70, Rhi71, Pin72b). The pulse sequence used here is actually a simplification of their reversing pulse sandwich.

The FIDs and echoes in the rigid lattice and in the rotationally fully narrowed region (i.e. where the line is temperature independent), could be fit with a simple gaussian at all except long times, where a weak (less than 5%) Lowe beat appears. In the regions of substantial motional narrowing the FIDs were exponential outside the receiver blocking.

At temperatures below 100 K the second moment has reached its low temperature limiting value of 27 $\pm$ 3 G^2. This is reasonable for the rigid lattice second moment of an organic solid. Indeed, Eguchi et al. (Egu75) have calculated the intramolecular part of the second moment as 16 G^2, averaging over the axial and equatorial molecular conformations.

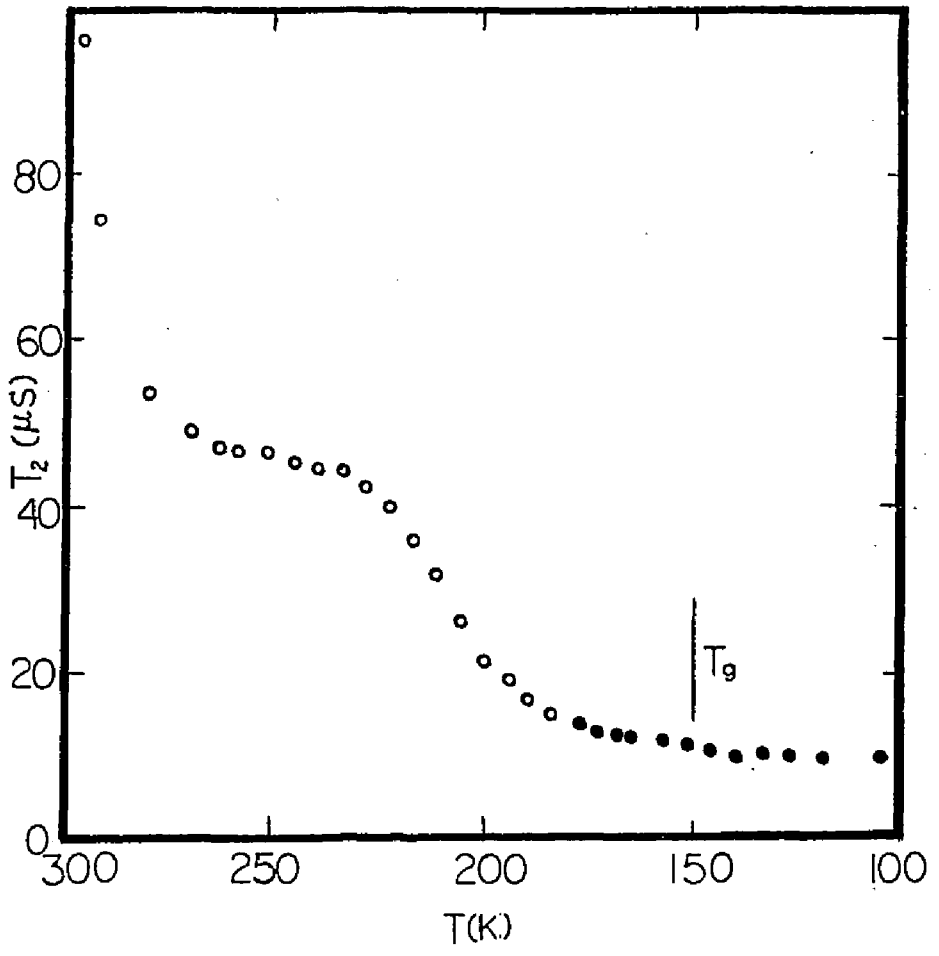

Figure 12: Proton T_2 values measured from FIDs (o) and solid echoes (•) in cyclohexanol. The increase in T_2 around 125 K is early narrowing (Tg = 150 K) due to the β motion.

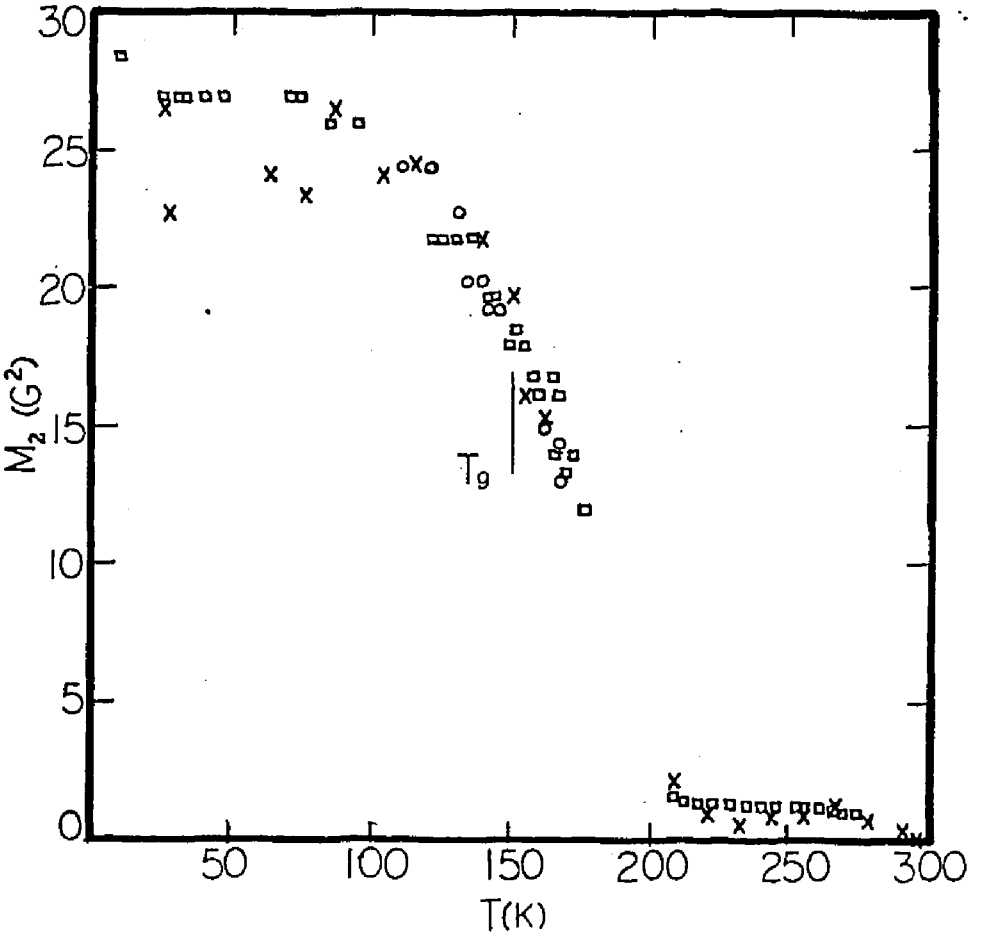

Figure 13: Proton M_2 determined from solid echoes (o) and magic echoes (□). The M_2 values (x) are from Eguchi's continuous wave measurements. The decrease in M_2 around 100 K is due to the β motion.

They estimated the intermolecular part as 8 G^2 from previous cyclohexane work (And53). Hence the observed low temperature second moment agrees reasonably with the predicted rigid lattice value of 24 G^2. We conclude that, below 100 K, all molecular rotational motions are slower than ~ 10^4 s^{-1} (the NMR rate scale).

Between 210 K and 275 K the observed second moment is approximately constant, 1.2 G^2. For the case of rapid molecular rotations, with no translational diffusion, the proton second moment is given by (Dmi64):

$$M_2 = (3/5)c\gamma^4h^2I(I+1)\sum_k(1/r_k)^6,$$

where it is assumed that all the spins of the molecule are located at its center, only like-spin interactions exist, and the sample is a powder. The number of spins per molecule c is 12 for cyclohexanol. The lattice sum over k, where k is the molecular index, has been evaluated for an fcc lattice as 115.63 a_o^{-6}, where a_o is the lattice spacing of cyclohexanol, 0.88 nm (Gre69b). The above equation gives the rotationally averaged second moment as 1.1 G^2, in reasonable agreement with the observed value. It should be noted that in many organic plastic crystals the rotationally averaged proton second moment is approximately 1 G^2 (Bod79). Since the FID in the rotationally averaged region is roughly gaussian, the observed T_2 of 45 μs is in accord with the observed M_2. Hence the observed linewidth in this region indicates that overall molecular rotation is occuring faster than ~ 10^4 s^{-1}.

Carbon-13 spectra at 20.85 MHz (natural abundance) for the liquid at T = 304 K and the solid at T = 286 K and 119 K are shown in Fig.

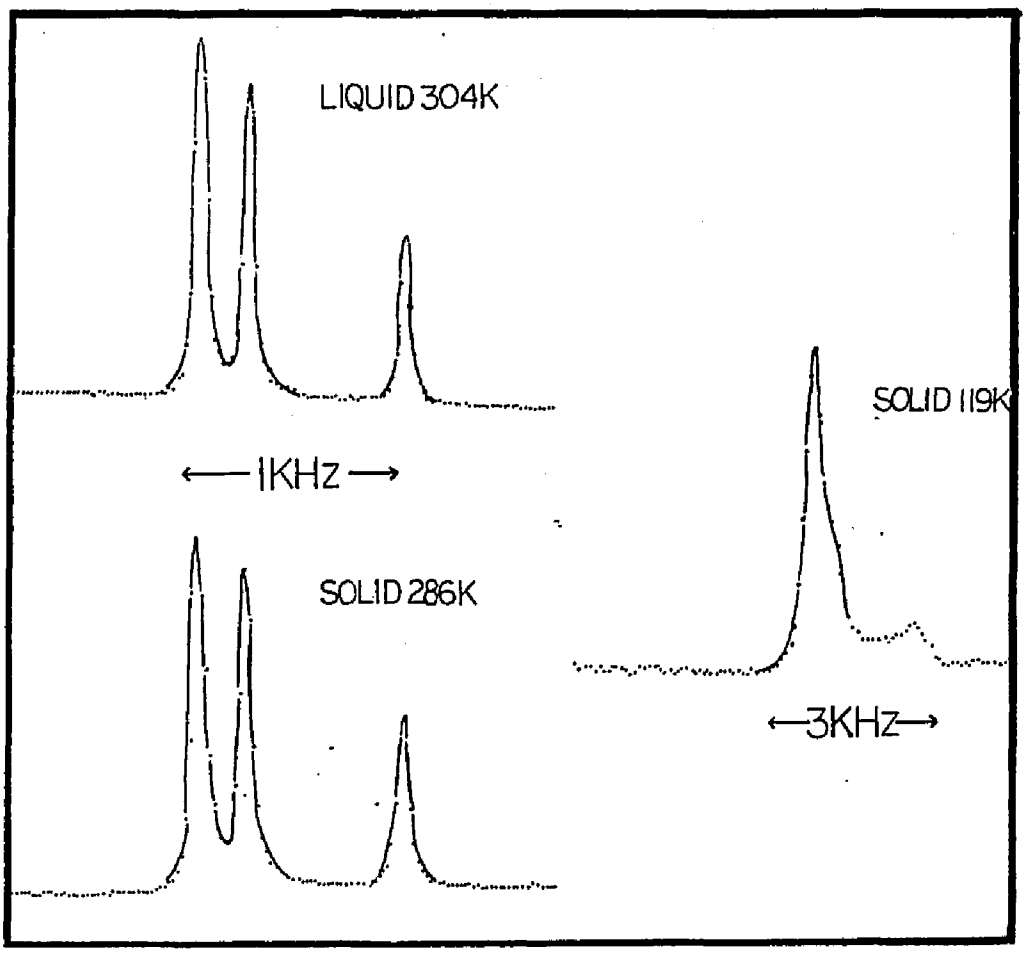

Figure 14: Carbon-13 spectra at three temperatures, one liquid at 304 K and two solid at 286K and 119 K. The high temperature solid and the liquid spectra are identical, indicating fast overall rotation in the solid.

15. The peak on the right is due to the OH carbon, the peak in the middle is due to the carbons adjacent to the OH carbon, and the peak on the left is due to the other three carbons. The solid spectrum shows the rigid lattice chemical shifts that are being averaged by the overall rotation. The spectra were taken using 23 ms of coherent spin-stirring (Meh71) ($\gamma H_1/2\pi$ = 80 KHz) and were digitally filtered with a Lorentzian of 40 Hz FWHM (Fuk81). For the solid spectra Hartmann-Hahn cross-polarization (Har62, Pin73) was used to enhance the C^{13} magnetization. The cross-polarization time was 1.9 ms. A 180 degree pulse was placed 650 μs after the beginning of the FID to refocus the C^{13} magnetization. The echo peak was fourier transformed to produce the solid spectra. The liquid spectrum and the warm solid spectrum are identical, implying that the rotational molecular motions in the high temperature solid are completely averaging the anisotropic part of the chemical shift tensor for all the carbons (Spi74a, Spi74b). At high temperatures the complete averaging of the anisotropic part of the chemical shift and the value of 1.2 G^2 for the second moment imply that the molecules are undergoing overall molecular rotation. Specifically, if θ is the angle between the magnetic field and any vector fixed in the molecule, the molecular motion averages $3\cos^2\theta - 1$ to zero. Free rotation is not implied, the volumes that are swept out by overall molecular rotation interpenetrate (Dun61).

Near the melt (299 K > T > 275 K) molecular translational diffusion is rapid enough to narrow the NMR line. As T increases towards the melt, T_2 becomes longer and the second moment goes towards zero (Egu75). The part of the intermolecular interaction which is not rota-

tionally averaged in the rotor crystal is averaged by the translational diffusion. However, the extent of narrowing before melting is not sufficient to allow the activation energy for diffusion to be extracted from T_2. In Fig. 15 the dipolar spin-lattice relaxation time T_{1D} also shows evidence of molecular translations above 245 K. This is the strong collision, slow motion regime treated by Ailion and Slichter (Ail71, Sli64). The jump time τ_j is essentially equal to T_{1D} here because there should be little site-to-site local field correlation. Setting $\tau_j = T_{1D}$ and fitting with an Arrhenius expression, we find $\tau_0 = 3.6 \times 10^{-13}$ s and (E/k) = 5550 K. This may be compared with the value 5000 K for translational activation energy measured in cyclohexane (Bod76), which melts at 280 K. In fact, rapid translational diffusion is common near the melt in rotor crystals (Bod79).

The existence of translational diffusion in solid cyclohexanol near the melt can be readily demonstrated. A sample of glassy crystal I formed by rapid cooling to 77 K is generally full of visible cracks and fractures. Upon warming to within two degrees of the melting temperature, the cracks in the sample will disappear in minutes as the sample anneals, indicating the presence of translational diffusion.

Both T_2 and M_2 in Figs. 12 and 13 show the onset of motional narrowing by 125 K. Narrowing at such a low temperture is surprising because the glass transition temperature (150 K) (Ada68) is generally where some important relaxation time becomes 10^3 s, much too slow to produce NMR line narrowing. The line narrowing below T_g is evidence for the existence of other motions faster than 10^{-4} s. We will return to these other motions later.

The relaxation time T_2 and the second moment M_2 are continuous functions of temperature. This is in accord with the view from calorimetric (Ada68), dielectric (Ada72), and X-ray experiments (Cec80) that the rotor crystal, supercooled crystal, and glassy crystal are all the same phase.

The spin-lattice relaxation time in the laboratory frame was measured by the conventional, saturate - wait - inspect, sequence (Blo48). The saturation pulse was usually a 400 μs pulse which saturated by virtue of H_1 inhomogeneity and transverse relaxation (T_2 is less than 400 μs). The inspection pulse was often a 90 degree pulse, but sometimes a solid echo sequence ($90_0-\tau-90_{90}$) (Low57) was used. The RF field strength was typically 80 KHz. The rotating frame relaxation time $T_{1\rho}$ was measured using the on resonance spin-locking pulse sequence ($90_0-\tau_{90}$) (Loo66). The dipolar relaxation time T_{1D} was measured using the Jeener - Broekaert pulse sequence ($90_0-t-45_{90}-\tau-45_0$) (Jee67).

For all temperatures and frequencies the T_1 recovery curves were exponential over the first decade. However the $T_{1\rho}$ and T_{1D} decay curves generally exhibited a small amount of non-exponentiality in the first decade. The times reported here represent inverse average relaxation rates, since the recoveries were fit at early times. The spin-relaxation times are plotted in Fig. 15 as a function of reciprocal temperature for all frequencies. T_1 and T_{1D} were measured at 21 MHz down to 5 K and appear in Fig. 16 as functions of temperature.

The most prominent feature in Fig. 15 is the existence of two T_1 minima, indicating that two relaxation mechanisms exist in cyclo-

hexanol I. The minima shift towards lower temperatures at lower frequencies, implying that the minima are due to thermally activated motions. The double minimum was also seen by Eguchi et al. (Egu75) in their proton T_1 measurements at 10 and 30 MHz. They attributed the double minimum to anisotropic overall rotation of the molecule. The correlation rate for rotation about the long axis was assumed to be markedly faster than about the other axes.

Adachi et al. (Ada72) studied the motion of the electric dipole moment (COH group) in cyclohexanol using dielectric spectroscopy at frequencies between 0.01 Hz and 300 KHz. They found two well resolved dielectric loss peaks. The prominent peak α was attributed to overall molecular rotation and the small peak β, 500 times weaker than the α peak, was called a secondary relaxation. The weakness of the β peak was explained by attributing it to OH group motion of a small fraction (~ 3%) of the molecules. Previous dielectric work at high frequencies reported only one dielectric loss peak, the α peak (Gre69a).

Motional minima of T_1 occur when $\omega\tau \sim 1$ (Sli80), where $\omega/2\pi$ is the NMR resonance frequency and τ is the correlation time of the motion. The frequency dependence of the temperature of each T_1 minimum is plotted along with dielectric data of Adachi et al. on the relaxation map, Fig. 17 (Ada72). In detail, it was assumed that $\omega_0\tau = 0.6$ at the T_1 minima ($\omega_0 = \gamma H_0$ and H_0 is the Zeeman field) and $\omega_1\tau = 0.5$ at the $T_{1\rho}$ minima ($\omega_1 = \gamma H_1$ and H_1 is the rf field). These are results of standard relaxation theories (Blo48, Loo66).

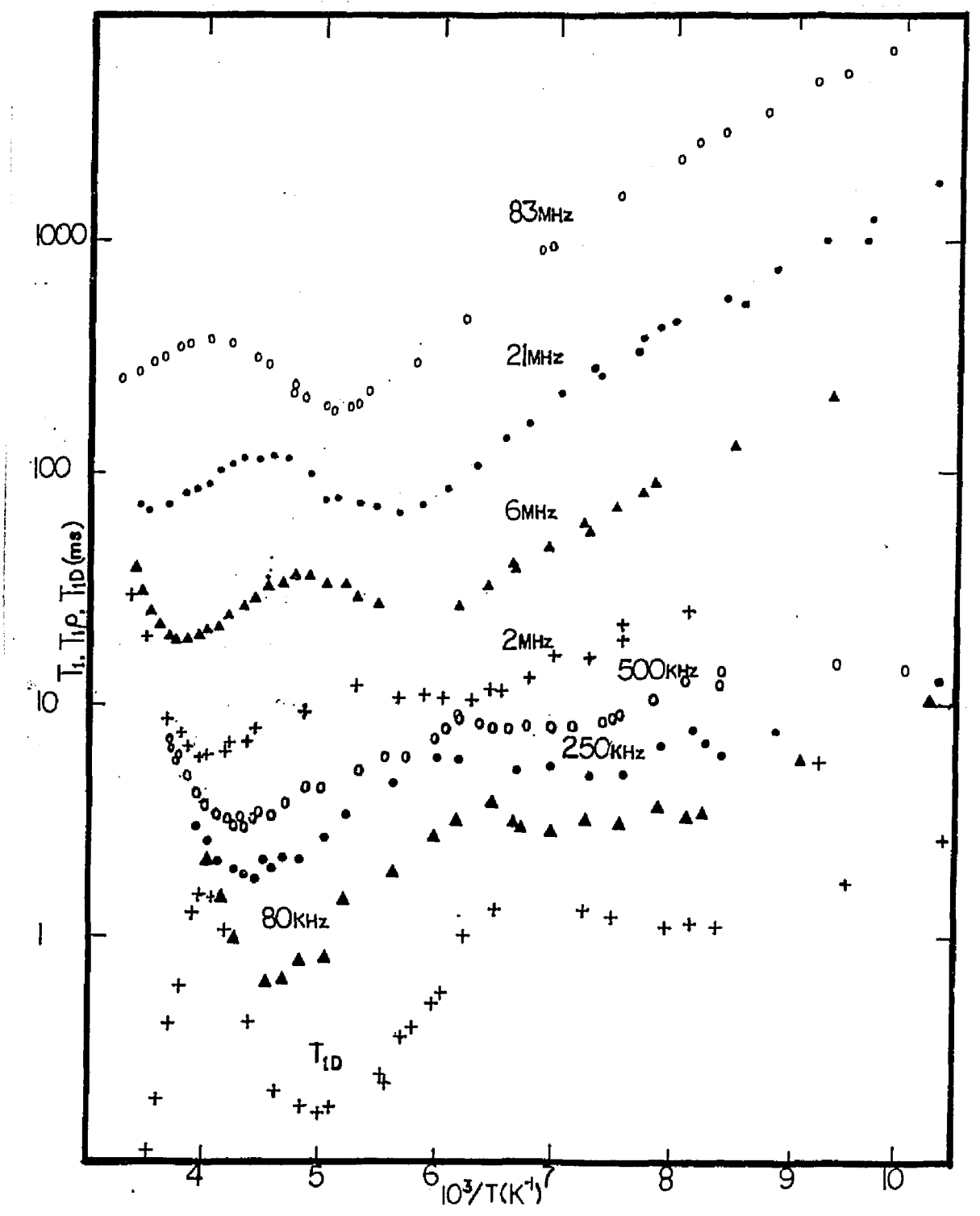

Figure 15: Spin-lattice relaxation times at various frequencies. The high temperature α minimum (left) is due to overall molecular rotation. The low temperature β minima is due to rotation of the cyclohexyl ring.

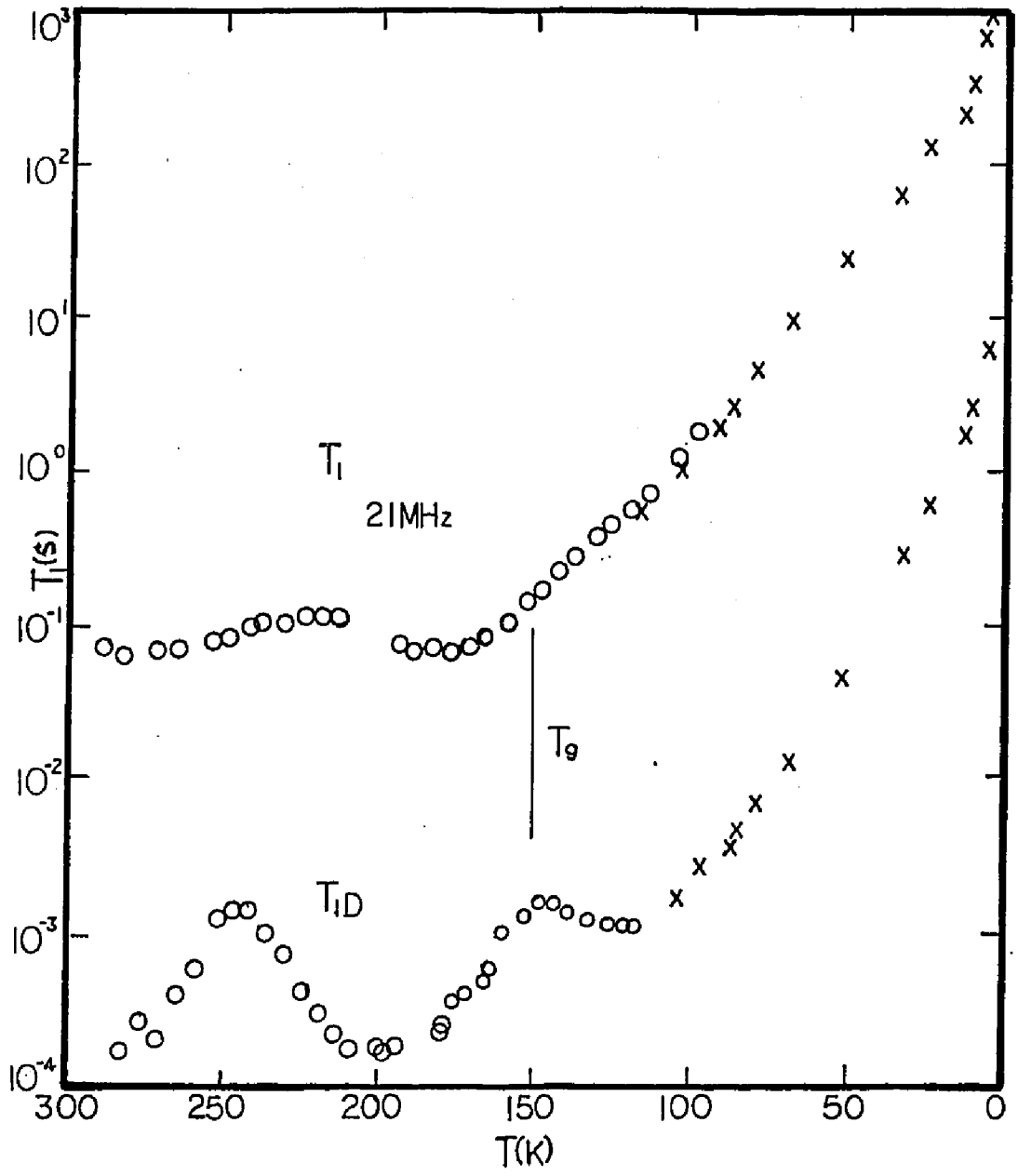

Figure 16: Spin-lattice relaxation times at 21 MHz and in the dipolar fields from 300 to 5 K.

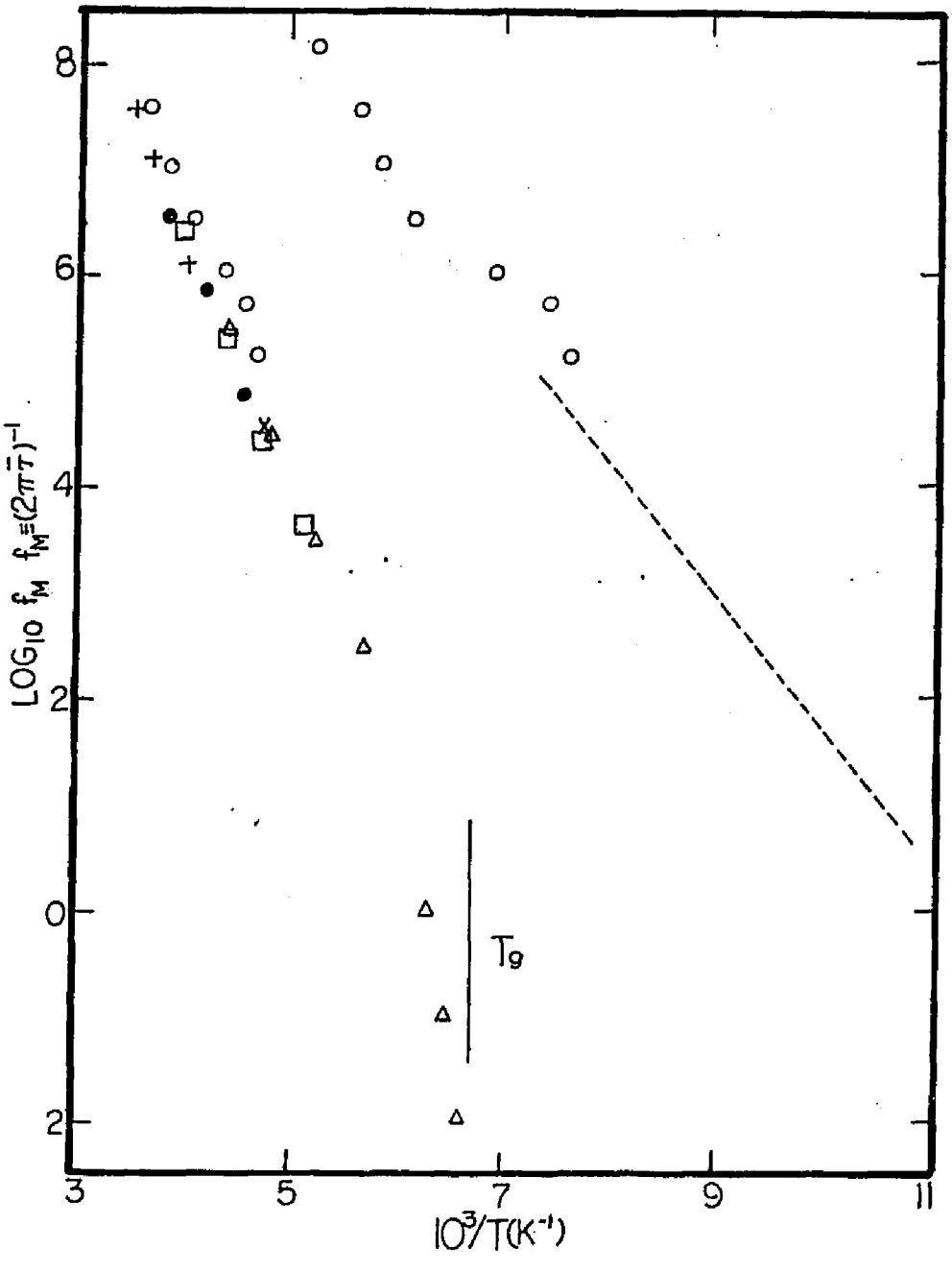

Figure 17: Motional frequencies in cyclohexanol shown for α motion, our T_1 minima (o) and dielectric data (x + • □ △) (Gre69b, Ada72), and for β motion our T_1 data (o) and dielectric data (---) (Ada72).

In the relaxation map, Fig. 17, the high temperature T_1 minima fall on a smooth curve adjacent to the α dielectric loss peaks and the low temperature T_1 minima fit on the β motion curve. Hence the two T_1 minima are due to the two motions previously observed dielectrically. The temperature dependence of the correlation times can be determined from the NMR - dielectric relaxation map. The α motion has a VTF or WLF temperature dependence given by (Wil55)

$$\tau(T) = \tau_0 \exp\left[(E/k)/(T - T_0)\right],$$

where $\tau_0 = 5.7 \times 10^{-13}$ s, $(E/k) = 1725$ K, and $T_0 = 95$ K. The T_0 value here is lower than suggested by the dielectric workers, but produces a better fit to all the data. The β motion correlation time has an Arrhenius temperature dependence given by

$$\tau(T) = \tau_0 \exp\left[(E/k)/T\right],$$

where $\tau_0 = 1 \times 10^{-15}$ s and $(E/k) = 2900$ K. The correlation time of the α motion extrapolates through $\tau = 10^3$ s at 147 K, near the calorimetric glass temperature of 150 K (Ada 68). This indicates that the freezing out of the α motion is indeed responsible for the glass transition observed in the specific heat. We note the α motion correlation rate (τ^{-1}) at the melt (299 K) is 5×10^8 s^{-1}. As mentioned previously, this is slow for a rotor crystal.

The substantial depth of the low temperature (β) T_1 minimum implies the β motion is a large motion that strongly modulates the proton dipolar interactions. For the high frequencies, the α and β T_1 minima are approximately the same depth. However we note that these

minima are not as deep as simple relaxation theory (BPP) for molecular rotation would predict. Later we will show that this is due to distributions of correlation times for both the α and β motions. Nevertheless, it is clear that both motions produce strong relaxation and must substantially modulate the proton dipolar interactions. The fraction of the rotationally averagable proton second moment modulated by the β motion cannot be deduced from T_2 or M_2, because the regions of narrowing due to the α and β motions overlap. However, a lower limit can be assigned to the fraction of the second moment that is averaged by the β motion by noting that any of the narrowing below T_g must be due entirely to the β motion. From Fig. 13 the early narrowing between 100 K and 150 K reduces M_2 from 27 G^2 to 18 G^2. Hence the β motion modulates at least 9 G^2 of the total 26 G^2 that is rotationally averagable. The α motion will start narrowing the NMR line when $\omega_M \sim 10^8\ s^{-1}$, from Fig. 17 this occurs at 167 K. Then from Fig. 13 the early narrowing (β motion) modulates 12 G^2 of the rotationally averagable second moment. Since the β motion modulates such a substantial fraction of the total second moment the β motion must be a large motion that involves essentially all the molecules. However in the dielectric study, the β relaxation peak was weak (Ada72). We conclude that the β motion is dielectrically quiet. That is the β motion leaves the permanent electric dipole moment fixed in the laboratory frame.

Any model of the dielectrically silent β motion must leave the molecular electric dipole moment fixed in space while substantially modulating the proton dipolar interactions. The dipole moment results primarily from the COH group and is parallel to neither the CO nor the OH

bond, but is roughly perpendicular to the CO bond in the COH plane (Hed77). Uniaxial overall molecular rotation about an axis parallel with the electric dipole moment would be dielectrically silent, but that seems unlikely. If the rotation axis passed through the COH group, the motion would sweep out an excessively large volume. Rotation about an axis that passes through the center of the ring, but is still parallel to the electric dipole moment, would involve large displacements of the COH group. This is unlikely in a hydrogen bonded network. Chair-chair and chair-boat interconversions also sweep out excessive volumes under the constraint of dielectric silence. The only reasonable motion that simultaneously satisfies the requirements of dielectric silence and large proton modulations is an internal rotation. It is a rotation of the cyclohexyl ring about the CO bond with the COH group held fixed. Since this involves rotation of the globlar part of the molecule (the ring), and not the hydrogen-bonding OH group, this motion is expected to be faster than overall molecular rotation (relaxation map, Fig. 17.) We do not speculate on the step-size or smoothness of this rotation.

Several features of the T_1 data imply the existence of distributions of correlation times of both the α and β motions (She79, Noa71).

i) The T_1 minima are not as deep as expected from relaxation theories, which assume a single exponential correlation function. For the case of isotropic rotation modulating a 26 G^2 second moment with an exponential correlation function, the minimum value of T_1 is 7.4 ms at 21 MHz. If one assumes that the α and β motions modulate equal fractions of the 26 G^2 rotationally averagable second moment, the minimum

values of T_1 are predicted to be 14.9 ms. The calculated temperature dependence of T_1 for this case appears in Fig. 18 along with the 21 MHz data.

The temperature dependence of the α and β single correlation times were taken from smooth fits to the data in the relaxation map, Fig. 17. The experimental T_1 minimum values are longer than the predicted values by a factor of ~ 4.3.

ii) The temperature dependence of the experimental T_1 is weaker than predicted in Fig. 18. In particular the slope of T_1 on the cold side of the β minimum corresponds to an activation energy of 760 K, much smaller than the 2900 K from the relaxation map. Similarly, the temperature dependence of T_{1D} on the cold side of the α minimum corresponds to a local activation energy ($d(\ln T_1)/d(1/T)$) of 1700 K, whereas the temperature dependence in the relaxation map is 4300 K. Hence, the slopes on the cold sides of both minima are smaller than expected. However, the 4300 K slope of T_{1D} and $T_{1\rho}$ on the hot side of the α minimum agrees with the 4300 K temperature dependence in the relaxation map. Thus, it appears that weaker than expected temperature dependences occur only on the cold sides of the minima.

iii) The frequency dependence of T_1 is not that expected for the case of exponential correlation functions. On the cold side of the β minimum at 110 K, T_1 is expected to vary as ω_0^2. The actual frequency dependence is $\omega_0^{1.2}$, as seen in Fig. 19. The $T_{1\rho}$ values in Fig. 19 were reduced by a factor of 2.1 to bring them into agreement with the T_1 values. This factor reflects the fact that a smaller part of the dipolar interaction is effective in rotating frame relaxa-

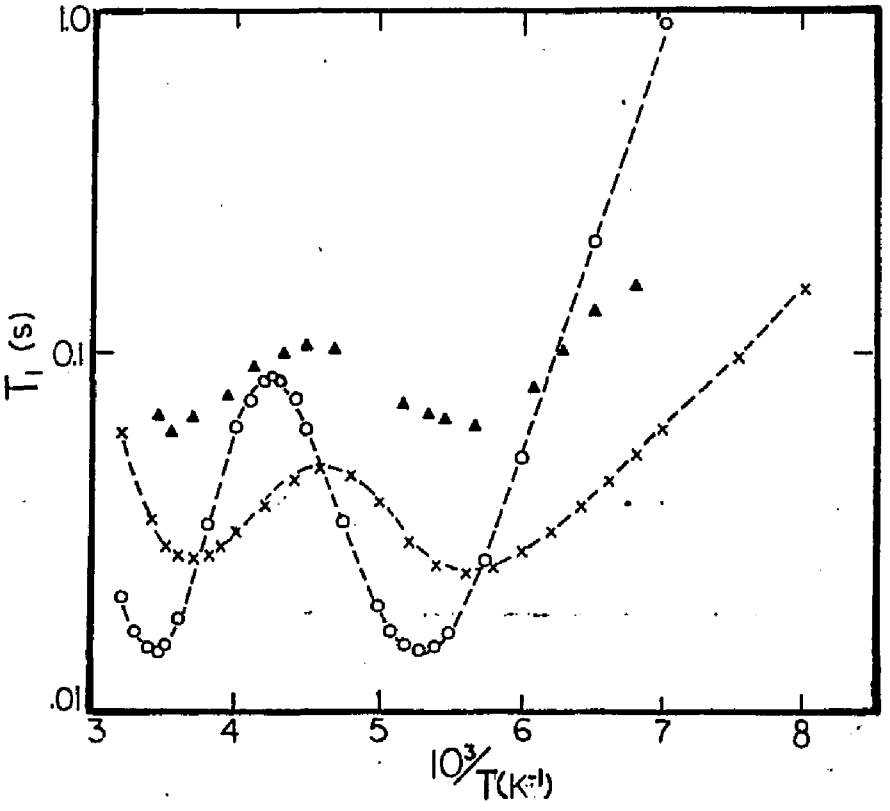

Figure 18: Comparison between our 21 MHz T_g data (▲), the results of BPP relaxation theory (o) (Blo48), and the results of C-D distributions (x) (Noa71), with a = 0.3 for both motions.

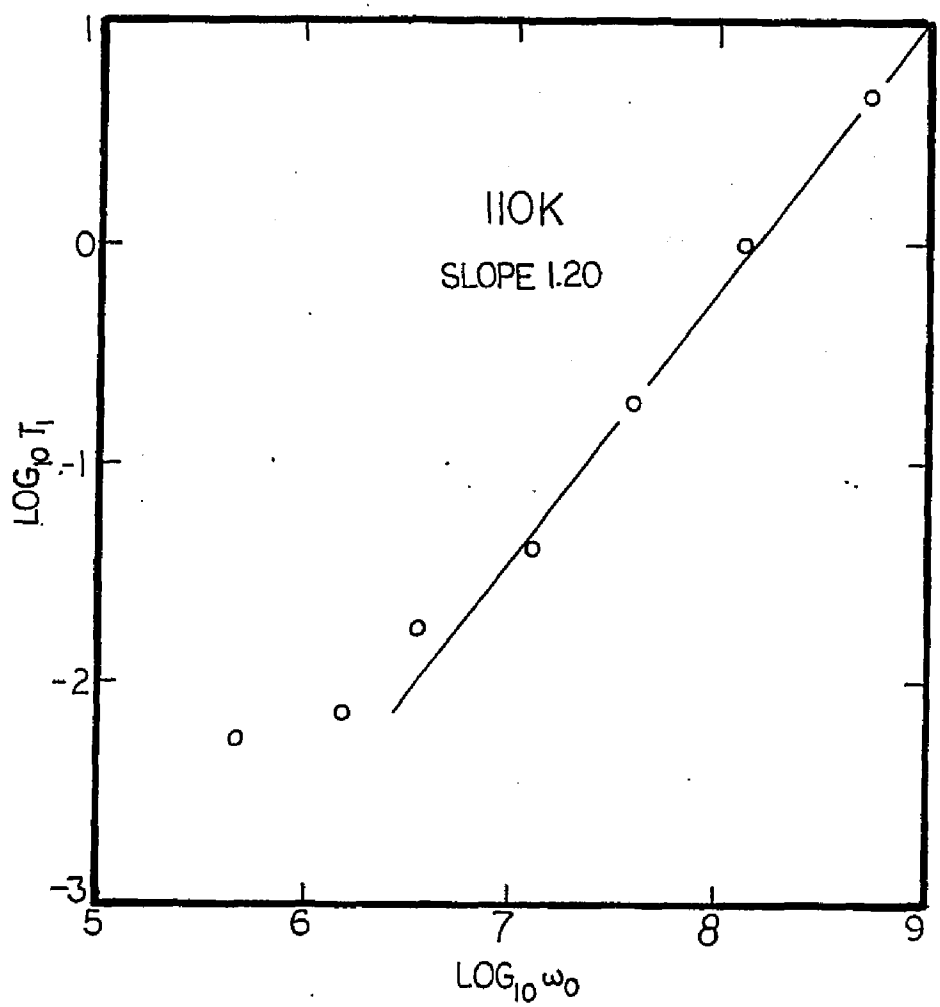

Figure 19: Frequency dependence of the spin-lattice relaxation times at 110 K. The slope of 1.2 indicates a distribution of relaxation times.

tion. The weak frequency dependence of T_1 and $T_{1\rho}$ indicates a distribution of β correlation times.

The frequency dependence of the minimum T_1 values at both minima are shown in Fig. 20. The α T_1 minimum values depend linearly on ω_0 or ω_1, after correction of the $T_{1\rho}$ values by the factor of 2.1. This linear dependence indicates only that the distribution of α correlation times has a temperature independent logarithmic width. However the minimum values of T_1 at the β minimum vary as $\omega_0^{0.78}$, indicating that the logarithmic width of the distribution of β correlation times becomes larger at low temperatures. This is also evident in Fig. 15, where the β minima appear less distinct at lower frequencies and temperatures.

The above observations indicate the existence of distributions of α and β correlation times. Noack (Noa71) has calculated T_1 for the case of a Cole-Davidson (Dav51b) distribution of correlation times.

$$g(\tau) = ((\sin a\pi)/\pi)(\tau/(\tau_0 - \tau))^a$$

for $\tau < \tau_0$

$$g(\tau) = 0$$

for $\tau > \tau_0$

using equation 36. We assumed that the α and β motions each modulate half of the 26 G^2 averageable moment and have C-D distributions of correlation times, with a = 0.3 (a = 1 is the limit of a single correlation time and a = 0 is an infinitely broad distribution). The relaxation

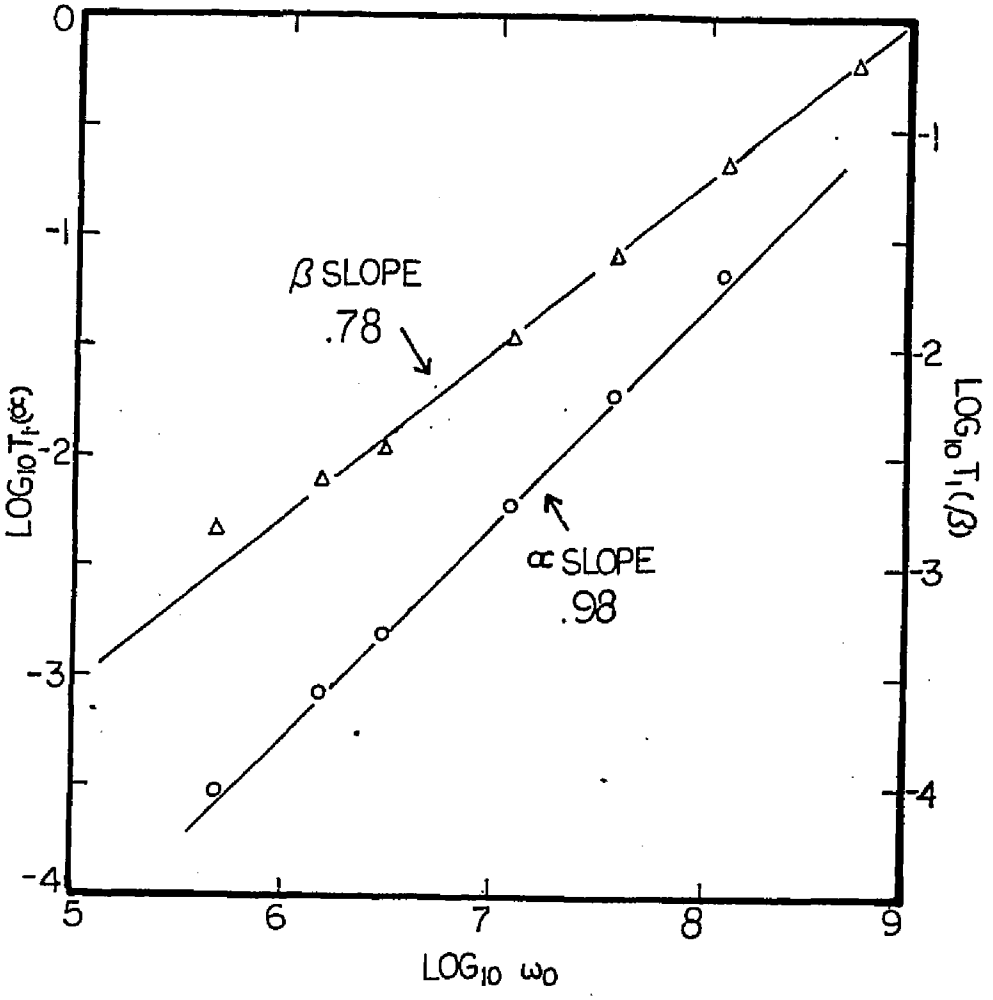

Figure 20: Frequency dependence of the spin-lattice motional minima. A slope of 1.0 indicates that the distribution is independent of temperature. The α motion has a slope of 1.0 and the β has a slope of 0.78.

map, Fig. 17, was used to obtain τ_0 values for the two motions. We note that τ_0 is at the edge of the distribution and it would have been more appropriate to take $\bar{\tau} = a\tau_0$ from Fig. 17. At each temperature, Noack's results were used to compute T_1. The results appear in Fig. 18. The computed minimum T_1 values are now larger, although still smaller than the experimental values by a factor of 2.3. The computed temperature dependence (aside from a multiplicative constant) is now in good agreement with the data. The frequency dependence of T_1 at 110 K is $\omega_0^{1.3}$, close to the observed $\omega_0^{1.2}$. Particular results of the C-D distribution are that the cold side frequency dependence is ω_0^{1+a} and that the local activation energy of T_1 on the cold side is just 'a' times the local activation energy describing the temperature dependence of τ_0. It appears impossible to adjust the parameters of our fit to obtain agreement with the minimum T_1 value while still giving the correct temperature dependence. The frequency and temperature dependences of T_1 on the cold side of the minimum reflect the short correlation time tail of the distributions. The minimum value of T_1 reflects instead the behavior of the distribution near its peak. It seems to us that a different form of distribution could give better agreement with the data. Nevertheless, the improvement in fit obtained by using the C-D distributions demonstrates that the motions in cyclohexanol-I do not have single correlation times. The observation that the minimum T_1 values are 4.3 times longer than predicted for the case of exponential correlation functions indicates that the distributions of correlation times are quite broad, regardless of the detailed shape of the distributions. This disagreement is in accord with the

dielectric data on the β loss peak (Fig. 13 of reference Ada72.) However, this is not in agreement with the α dielectric loss peak data, which is at least roughly described by a single correlation time. Unfortunately, Cole-Cole plots of the α peak were not presented. This may indicate that the α motion is more narrowly distributed than we have proposed, but modulates a smaller fraction of the rotationally averageable second moment.

We turn now to the T_1 data below 100 K. Our first measurements were on a sample evidently contaminated with O_2. Its T_1 was essentially independent of temperature below 70 K (Fuk81, Blo48). The data in Fig. 16 refer to a sample prepared by bubbling He gas through it to strip away the dissolved O_2. The substantial temperature dependence of T_1 in Fig. 16 indicates that O_2 was not a problem in this sample. The temperature variation of T_1 and T_{1D} appear to be smooth continuations of the higher temperature data. The frequency dependence can be extracted crudely from the ratio of T_1 and T_{1D}, knowing the ratio of relevant frequencies is 1650 (21 MHz to 13 KHz = $(2\pi)^{-1}\gamma H_L$, where H_L is the local field) (Sli61). The ratio of T_1/T_{1D} ranges from 550 at 60 K to 140 at 5 K. This indicates, although only in a <u>most</u> preliminary way, a less than ω_0^2 dependence on T_1. Fast motions are necessary to obtain a T_1 frequency dependence that is weaker than ω_0^2. Therefore there exist some motions, or a tail of a distribution of motional rates, faster than ω_0 even at 5 K. However it would be surprising if the tail of the β motion correlation time distribution could determine T_1 at 5 K. The possible role of tunneling centers in determining T_1 at low temperatures is not clear. These curi-

ous results (short T_1 and weak temperature and frequency dependences of T_1) call for a more thorough study at low temperatures.

We note that in disordered materials these reduced temperature and frequency dependences have been seen before. Walstedt et al. (Wal77) found in their measurements on Na^{23} at two frequencies in the ionic conductor Na-β alumina, that T_1 had a weak temperature and frequency dependence due to ion hopping. They interpreted these results as arising from a distribution of relaxation times for ion hopping. (Bjorkstram et al. saw the same T_1 dependences is their Na-β alumina work. They interpreted it as evidence for 2-D motion.) (Bjo81) Stokes and Ailion, in their spin-lattice relaxation (^{19}F) study of the molecular motions in $C_2F_2Cl_4$ (1,2-difluorotetrachloroethane), another rotor crystal that can be supercooled, found weaker than expected temperature and frequency dependences for T_1 and $T_{1\rho}$ (Sto79). They speculated that these effects could be due to a distribution of relaxation rates.

5.4 CYCLOHEXANOL CONCLUSIONS

We find that the molecular motions in solid cyclohexanol, a rotor crystal that forms an orientational glass upon supercooling, are not as simple as was previously thought based on experiments by X-ray, calorimetric (Ada68) and dielectric techniques (Ada72). The previous view held that all the molecular motions ceased on laboratory time scales below T_g (150 K). Instead, we find from proton NMR that there exist two important rotational motions in the solid rotor phase one of which extends below T_g. The complete averaging seen by proton and carbon-13 NMR

in the warm solid indicates that the α motion is overall molecular rotation. The value of the spin relaxation times and the weak dielectric loss peak associated with the β motion indicate that it is an internal rotation of the cyclohexyl ring about the CO bond with the COH group held fixed, not a uniaxial overall molecular rotation as suggested by other NMR workers (Egu75). We find that even at T_g, where the α rotational correlation time is approximately 10^3 s, considerably faster motions exist in the glassy crystal as seen from our measurement of T_2 and M_2 and the low values of T_1.

The α and β motions each are described by distributions of correlation times as indicated by the shallow T_1 minima and the weak temperature and frequency dependences of T_1. The distribution of β correlation times becomes broader at low temperatures, so much so that the minimum in $T_{1\rho}$ at low frequencies associated with the β motion becomes indistinct.

The weak temperature dependence of T_1 extends from just below T_g down to low temperatures. This indicates that there are still parts of the distribution of motional rates faster than ~ 1 MHz, even at 5 K. The nature of the motion responsible for the low temperature spin relaxation is not known.

Chapter VI

CONCLUSIONS

We studied the molecular motions in two organic glass formers, glycerol and cyclohexanol. Glycerol is a liquid glass former, the more conventional type of glass. It is both orientationally and translationally disordered. Cyclohexanol is an orientational glass former, that forms from a rotor crystal. It posesses only orientational disorder.

The glycerol experiments used the slow motion technique of spectral hole-burning (Con81), which uses the anisotropic chemical shift and should be applicable to any NMR line which is inhomogenously broadened by chemical shift anisotropy. This includes the C^{13} spectra of almost all organic solids, including many polymers, provided the protons are spin-stirred. Following the hole recovery reveals the step-size of the molecular reorientations of both the molecules and the functional groups. This is a more detailed description of the rotational motions than is possible using other relaxation techniques.

In the experiments on supercooled glycerol the reorientation rates were followed from $10^{-2}s^{-1}$ to $10^{2}s^{-1}$ just above T_g. Our determination of the reorientation rate fit smoothly onto higher frequency NMR and dielectric determinations and extrapolate through 10^{3} s very near the calorimetric glass termperature. The mean angular reorientation was found to be large angle jumps, greater than 45 degrees, in agreement with the findings of the previous workers.

The experiments on cyclohexanol were done using conventional NMR relaxation techniques to study an interesting form of disorder, intrinsic (unforced) orientational disorder.

Two rotational motions were observed, one of which freezes out at the glass transition, the other persists to well below T_g(150 K). The glassing motion was determined to be overall molecular rotation from the liquid-like carbon-13 spectra in the high temperature solid and from the value of the plateau in M_2 at high temperatures. The surprizing result was that any motion persisted on slow NMR time scales (> 100 KHz) below T_g. This accounts for the weak relaxation peak seen by the dielectric workers, who interpreted it as OH group motion on a small fraction of the molecules (3%). Another NMR study attributed this motion to anisotropic molecular rotation, which would give large dielectric signals.

The motions studied in both samples had distributions of correlation times a situation common in disordered materials. The recovery of holes in glycerol could be fit using the Williams-Watts function with $\beta = 0.5$. The spin-lattice relaxation times measured in cyclohexanol had weak temperature and frequency dependences indicating there exist distributions of relaxation times for both motions. The width of these distributions were found to be independent of temperature in glycerol and in the overall molecular rotation in cyclohexanol. However the logarithmic width of the internal motion in cyclohexanol was found to increase for decreasing temperature. In fact, because of the weak temperature and frequency dependence even down to 5 K, it appears that there exists a distribution of correlation times at these low temperatures.

That the tail of the distribution of correlation times of the internal motion extends to 5 K seems unlikely, perhaps T_1 is being influenced by tunneling.

The study of molecular motions in disordered materials is filled with many instances of interesting behavior that will remain a source of fruitful study for years to come, for the experimentalist, the theoretician and for industry.

REFERENCES

Abr78 A. Abragam, The Principles of Nuclear Magnetism, Oxford (1978).

Abr58 A. Abragam and W.G. Proctor, Phys. Rev., 109, 1441 (1958).

Ada68 K. Adachi, H. Suga, S. Seki, Bul. Chem. Soc. Japan, 41, 1073 (1968).

Ada72 K. Adachi, H. Suga, S. Seki et al., Mol. Cryst. Liq. Cryst., 18, 345 (1972).

Ail71 D.C. Ailion, Advances in Magnetic Resonance, Vol. 5, edited by J.S. Waugh, Academic Press (1971).

And53 E.R. Andrew, R.G. Eades, Proc. Roy. Soc., A218, 537 (1953).

And62 A.G. Anderson and S.R. Hartmann, Phys. Rev., 128, 2023 (1962).

Bjo81 J.L. Bjorkstam, M. Villa, and G.C. Farrington, Proceedings of the International Conference on Fast Ionic Transport in Solids, edited by J.B. Bates and G.C. Farrington, North-Holland Publishing Co. (1981), p.153.

Blo46 F. Bloch, Phys. Rev., 70, 460 (1946).

Blo48 N. Bloembergen, E.M. Purcell, and R.V. Pound, Phys. Rev., 73, 679 (1948).

Blo53 N. Bloembergen and T.J. Rowland, Acta Metallurgica, 1, 731 (1953).

Bod79 N. Boden in The Plastically Crystalline State, edited by J.N. Sherwood, John Wiley & Sons (1979).

Bod76 N. Boden, J. Cohen, and R.T. Squires, Mol. Phys., 31, 1813 (1976).

Bow82 R.C. Bowman Jr. and W. Rhim, J. Magn. Res., 49, (1982).

Car54 H.Y. Carr and E.M. Purcell, Phys. Rev., 94, 630 (1954).

Car53 T.R. Carver and C.P. Slichter, Phys. Rev., 92, 212 (1953).

Car56 T.R. Carver and C.P. Slichter, Phys. Rev., 102, 975 (1956).

Cec80 D. Ceccaldi, F. Denoyer, M. Lambert, and H. Szware, J. Phys. Lettres, 41, L-365 (1980).

Con77 M.S. Conradi, Rev. Sci. Instrum., 48, 359 (1977).

Con81 M.S. Conradi and P.L. Kuhns, Bull. Am. Phys. Soc., 26, 219 (1981).

Cro76 V.R. Cross, R.K. Hester, and J.S. Waugh, Rev. Sci. Instrum., 47, 1486 (1976).

Dav51a D.W. Davidson, R.H. Cole, J. Chem. Phys., 19, 1417 (1951).

Dav51b D.W. Davidson and R.H. Cole, J. Chem. Phys., 19, 1484 (1951).

Dem73 C. Demau and G. Vicq, C. R. Acad. Sci. Paris B, 276, 369 (1973).

Dem74 C. Demoulin, C.J. Montrose, and N. Ostrowsky, Phys. Rev. A, 9, 1740 (1974).

Die69 P. Diehl and C.L. Kheptrapal, NMR: Basic Principles and Progress, Vol. 1, Springer, (1969).

Dmi64 L.V. Dmitrieva and V.V. Moskalev, Sov. Phys. Solid State, 5, 1623 (1964).

Dun61 W.J. Dunning, J. Phys. Chem. Solids, 18, 21 (1961).

Ear79 W.L. Earl and D.L. VanderHart, Macromolecules, 12, 762 (1979).

Egu75 T. Eguchi, G. Soda, and H. Chihara, J. Magn. Res., 23, 55 (1975).

Fuk81 E. Fukushima, S.B.W. Reeder, Experimental Pulse NMR: A Nuts and Bolts Approach, Addison-Wesley Publishing Co. Inc. (1981).

Gib23 G.E. Gibson, W.F. Giauque, J. Am. Chem. Soc., 45, 93 (1923).

Gre69a J.R. Green, W.T. Griffith, Mol. Cryst. Liq. Cryst., 6, 23 (1969).

Gre69b J.R. Green, D.R. Wheeler, Mol. Cryst. Liq. Cryst., 6, 13 (1969).

Hah50 E.L. Hahn, Phys. Rev., 80, 580 (1950).

Har62 S.R. Hartman, E.L. Hahn, Phys. Rev., 128, 2042 (1962).

Hed77 P. Hedvig, Dielectric Spectroscopy of Polymers, John Wiley and Sons (1977).

Jee68 J. Jeener in Advances in Magnetic Resonance, Vol. 3, edited by J.S. Waugh, Academy Press (1968).

Jee67 J. Jeener, P. Brocker, Phys. Rev., 157, 232 (1967).

Jon67 G.P. Jones and J.T. Oaycock, Phys. Lett., 24A, 302 (1967).

Kan80 S. Kan, M. Fan, and J.Cortieu, Rev. Sci. Instrum., 51, 887 (1980).

Kel29 K.K. Kelly, J. Am. Chem. Soc., 51, 1400 (1929).

Kuh82 P.L. Kuhns and M.S. Conradi, J. Chem. Phys., 77, 1771 (1982).

Lau80 M. Lausch, H.W. Spiess, Cehm. Phys. Lett., 71, 182 (1980).

Lin80 C.P. Lindsay, G.D. Patterson, J. Chem. Phys., 73, 3348 (1980).

Lit63 T.A. Litovitz and G.E. McDuffie Jr., J. Chem. Phys., 39, 729 (1963).

Loo66 D.C. Look, I.J. Lowe, J. Chem. Phys., 44, 2995 (1966).

Low57 I.J. Lowe and R.E. Norberg, Phys. Rev., 107, 46 (1957).

McC67 N.G. McCrum, B.E. Read, and G. Williams, Anelastic and Dielectric Effects in Polymeric Solids, Wiley (1967).

McD62 G.E. McDuffie Jr., and T.A. Litovitz, J. Chem. Phys., 37, 1699 (1962).

McD63 G.E. McDuffie Jr., R.G. Quinn, and T.A. Litovitz, J. Chem. Phys., 39, 239 (1963).

Meh76 M. Mehring in NMR: Basic Principles and Progress, Vol. 11, edited by P. Diehl, E. Fluck, and R. Kosfeld, Springer-Verlag (1976). bib Meh71 M. Mehring, A. Pines, W. Rhim, and J.S. Waugh, J. Chem. Phys., 54, 3239 (1971).

Mei58 S. Meiboom and D. Gill, Rev. Sci. Inst., 29, 688 (1958).

Mor34 S.O. Morgen, Electrochem. Soc., 65, 109 (1934).

Noa71 F. Noack in NMR: Basic Principles and Progress, Vol. 3, edited by P. Diehl, E. Fluck, R. Kosfield, Springer-Verlag (1971).

Noa67 F. Noack and G. Preissing in Magnetic Resonance and Relaxation, edited by R. Blick, North-Holland (1967), p.104.

Nor82 R.E. Norberg, private communication (1982).

ORe72 D.E. O'Reilly, E.M. Peterson, and D.L. Hogenboom, J. Chem. Phys., 57, 3969 (1972).

Ots55 A. Otsubo and T. Sugawara, Sci. Rep. Res. Inst. Tohoku Univ., A7, 583 (1955).

Ove53a A.W. Overhauser, Phys. Rev., 91, 476 (1953).

Ove53b A.W. Overhauser, Phys. Rev., 92, 411 (1953).

Par27 G. Parks and H. Huffman, J. Phys. Chem., 31, 1842 (1927).

Pin71 A. Pines, M.G. Gibby, and J.S. Waugh, J. Chem. Phys., 56, (1971).

Pin72a A. Pines, M.G. Gibby and J.S. Waugh, Chem. Phys. Letters, 15, 373 (1972).

Pin73 A. Pines, M.G. Gibby, J.S. Waugh, J. Chem. Phys., 59, 569 (1973).

Pin72b A. Pines, W. Rhim, and J.S. Waugh, J. Magn. Res., 6, 457 (1972).

Pin68 D.A. Pinnow, S.J. Candau, and T.A. Litovitz, J. Chem. Phys., 49, 347 (1968).

Ram50 N.F. Ramsey, Phys. Rev., 78, 699 (1950).

Ram52 N.F. Ramsey, Phys. Rev., 86, 243 (1952).

Ram56 N.F. Ramsey, Phys. Rev., 103, 20 (1956).

Red55 A.G. Redfield, Phys. Rev., 98, 1787 (1955).

Res69 H.A. Resing, Mol. Cryst. Liq. Cryst., 9, 101 (1969).

Rhi70 W. Rhim, A. Pines, and J.S. Waugh, Phys. Rev. Lett., 25, 218 (1970).

Rhi71 W. Rhim, A. Pines, and J.S. Waugh, Phys. Rev. B, 3, 684 (1971).

Ric57 R. Riccirelli and T.A. Litovitz, J. Acoust. Soc. Am., 29, 1009 (1957).

Rot81 W.P. Rotwell and J.S. Waugh, J. Chem. Phys., 74, 2721 (1981).

Sch77 J. Schaefer, E.O. Stejskal, and R. Buchdahl, Macromolecules, 10, 384 (1977).

Sch68 L.I. Schiff, Quantum Mechanics, Third Ed., McGraw-Hill (1968).

Sli80 C.P. Slichter, Principles of Magnetic Resonance, Springer-Verlag (1980).

Sli64 C.P. Slichter and D. Ailion, Phys. Rev., 135, A1099 (1964).

Sli61 C.P. Slichter and W.C. Holton, Phys. Rev., 122, 1701 (1961).

Sod74 G. Soda, H. Chihara, J. Phys. Soc. Japan, 36, 954 (1974).

Spi74a H.W. Spiess, Chem. Phys., 6, 217 (1974).

Spi80 H. Spiess, J. Chem. Phys. 72, 6755 (1980).

Spi74b H.W. Spiess, R. Groseseu and U. Haeberlen, Chem. Phys., 5, 225 (1974).

Ste75 E.O. Stejeskal and J. Schaefer, J. Magn. Res., 18, 560 (1975).

Ste73 J. Stepisnik and J. Slak, J. Magn. Res., 12, 148 (1973).

Sto79 H.T. Stokes, T.A. Case, and D.C. Ailion, J. Chem. Phys., 70, 3563 (1979).

Str64 R.L. Strombotne and E.L. Hahn, Phys. Rev., 133, A1616 (1964).

Sug81 H. Suga, private communication (1981).

Suw80 D. Suwelack, W.P. Rothwell, and J.S. Waugh, J. Chem. Phys., 73, 2559 (1980).

Tim61 J. Timmermans, J. Phys. Chem. Solids, 18, 1 (1961).

Van48 J.H. Van Vleck, Phys. Rev., 74, 1168 (1948).

Van79 D.L. VanderHart and A.N. Garroway, J. Chem. Phys., 71, 2773 (1979).

Vol78 K.W. Vollmer, I.J. Lowe, and M. Punkkinen, J. Magn. Res., 30, 33 (1978).

Wal77 R.E. Walstedt, R. Dupree, J.P. Remeika, and A. Rodriguez, Phys. Rev. B, 15, 3442 (1977).

Wil155 M.L. Williams, R.F. Landel, and J.D. Ferry, J. Am. Chem. Soc., 77, 3701 (1955).

Wil70 G. Williams and D.C. Wats, Trans. Farraday Soc., 66, 80 (1970).

Wil71 G. Williams, D.C. Watts, S.B. Dev, Trans. Farraday. Soc., 67, 1323 (1971).

Wol79 M. Wolfe and J. Jones, J. Chem. Phys., 71, 3252 (1979).

TABLE

LIST OF FIGURES